IAS (2025) Nucleation and growth of sedimentary minerals, 396-420

From the rock to the precursor: sedimentary iron and manganese minerals as records of an evolving early Earth

HARILAOS TSIKOS[1,2*] CLANCY Z. JIANG[3], ROSALIE TOSTEVIN[4], XOLANE R. MHLANGA[5], ANSAHMBOM Y. NKE[4], MEHRNAZ SIAHI[6] and PAUL R.D. MASON[7]

[1]*Department of Geology, University of Patras, GR-26504 Rio, Greece; and,*
[2]*Department of Earth Sciences, Stellenbosch University, Private Bag X1, Matieland 7602, South Africa*
[3]*Department of Earth Sciences, University of Cambridge, CB2 3EQ England, United Kingdom*
[4]*Department of Geosciences, University of Cape Town, Rondebosch 7700, South Africa*
[5]*School of Biology and Environmental Sciences, University of Mpumalanga, Nelspruit 1201, South Africa*
[6]*Department of Geological Sciences, Missouri University of Science & Technology, Rolla, MO65409, USA*
[7]*Department of Earth Sciences, Utrecht University, Princetonlaan 8A, 3584CB Utrecht, the Netherlands*

**Corresponding author: htsikos@upatras.gr, htsikos@gmail.com*

ABSTRACT

Authigenic sedimentary iron and manganese deposits are key archives of the redox evolution of the atmosphere-ocean system, with potential to elucidate major events in deep time, such as the onset of oxygenic photosynthesis and the Great Oxidation Event. This review identifies iron formations and Mn-rich sedimentary rocks, straddling the time interval 2.7 to 2.0 Ga, as the part of the geological record that can best inform current debates on the evolution of oxygen on the early Earth. The links between the present-day composition of these rocks, as affected by diagenesis and metamorphism, and the precursor mineralogy which formed in the primary depositional environment, are explored. The current theories are then critically discussed together with evidence for transient oxygenation events under anoxic conditions prior to global oxygenation (O_2 oases and "whiffs") and Fe and Mn redox and Mn deposition across the Great Oxidation Event. It is possible to conclude, through ongoing and rigorous consideration of geochemical mass balance, mineralogical and textural heterogeneity and mineral-specific geochemistry, that Fe-rich and Mn-rich sedimentary deposits provide one of the best archives of the redox evolution of stratified marine environments in deep time.

Keywords: Great Oxidation Event, iron, manganese, mineralogy, redox

READING THE EARLY PRECAMBRIAN RECORD OF SEDIMENTARY FE AND MN DEPOSITS

Iron and manganese are two of the most abundant transition metals in the Earth's crust, sharing a similar redox chemistry in near-surface aqueous environments. Both elements are relatively soluble in their reduced, divalent state (Fe^{2+} and Mn^{2+}), whilst they form insoluble high-valence (oxyhydr)oxides [$Fe^{3+}(OH)_3$, $Fe^{3+}{}_2O_3$; $Mn^{3+}OOH$, $Mn^{4+}O_2$] under more oxidizing conditions (Canfield *et al.*, 2005). Given this chemical basis, enrichments in Fe and/or Mn in Precambrian chemical sediments provide a potentially valuable archive of biogeochemical redox evolution of the ocean-atmosphere system through deep time. The onset of oxygenic photosynthesis in the Archaean followed by the Great Oxidation Event (GOE) at *ca.* 2.4-2.0 Ga are key events that should have had a major impact on Fe- and Mn-geochemistry. Despite this, the relationship between the modelled oxygenation of the atmosphere across this time interval and the abundance and mineralogy of Fe and Mn in rocks of the same age has proven to be complex (*e.g.*, Bekker *et al.*, 2010, 2013; Lyons *et al.*, 2014; Planavsky *et al.*, 2014; Fischer *et al.*, 2015; Johnson *et al.*, 2013; Thibon *et al.*, 2019;

Hummer *et al.*, 2022).

Although Fe-rich sedimentary rocks occur throughout the geological record, arguably the most significant of these in the context of the early coevolution of oxygen and life are the so-called "iron formations", also widely referred to in the literature by the acronym "IF" (reviewed in Bekker *et al.*, 2010, 2013; and Konhauser *et al.*, 2017). These are defined as siliceous sedimentary rocks containing a minimum of 15 wt% Fe (James, 1954) with negligible input of external detrital material. Most IF are characteristically banded on various scales and hence are referred to as "BIF", but varieties dominated by granular textures also exist, termed "GIF" (Bekker & Kovalick, 2021). Deposition of IF occurred throughout the first half of Earth history, starting as relatively localised, small-volume and often hydrothermally controlled occurrences in the Eoarchaean (Algoma-type; *e.g.*, Mloszewska *et al.*, 2013; Nutman *et al.*, 2017; see also Fig. 1). Iron formation deposition reached a major peak during the period 2.7-2.4 Ga, epitomised by some of the spatially and stratigraphically most extensive epicratonic sedimentary IF (Superior-type; see Fig. 1), including the Hamersley Supergroup, Australia, Transvaal/Griqualand West Supergroups, South Africa, and Minas Gerais Supergroup, Brazil (Bekker *et al.*, 2010). The relative abundance of IF declined sharply after the GOE, with notable exceptions being a peak during the late Palaeoproterozoic (*ca.* 1.8-1.9 Ga), before a final stage of widespread deposition in the Neoproterozoic (Rapitan IF, Konhauser *et al.*, 2017; see Fig. 1).

Iron, as both Fe^{2+} and Fe^{3+}, is hosted in a range of mineral phases in unmetamorphosed IF, such as the dominant Fe oxide magnetite, the silicate minerals greenalite, minnesotaite, stilpnomelane and riebeckite, the carbonates siderite and ankerite, and much less common Fe sulphides (Table 1; Klein, 2005). Abundant microcrystalline quartz co-occurs with the Fe assemblages, whilst minor calcite and apatite are occasionally present. Haematite also occurs in IF and has been variably interpreted as either a primary (*e.g.*, Beukes, 1983) or secondary phase (*e.g.*, Rasmussen *et al.*, 2016). Its significance is explored further below.

The assemblage of minerals found in IF and outlined above not only reflects primary precipitation but also diagenetic recrystallization. Diagenesis is thought to alter the mineralogy partially or completely during rock formation (*e.g.*, Konhauser *et al.*, 2005). Further to this, many IFs are metamorphosed resulting in additional mineralogical transformations. Higher metamorphic grades lead to the formation of minerals such as Fe amphiboles (*e.g.*, grunerite), Fe pyroxenes, and/or Fe olivine (fayalite) at the

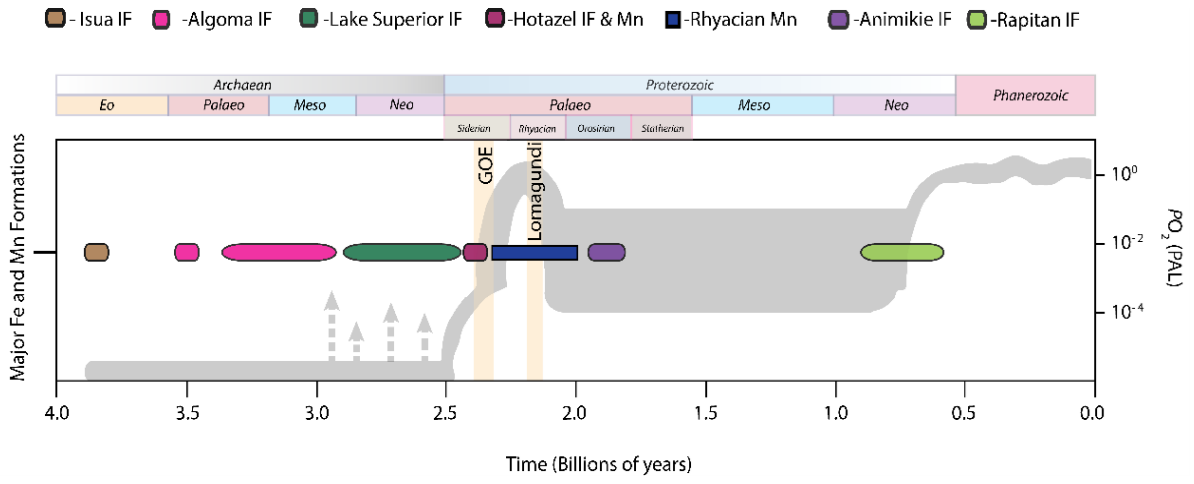

Fig. 1. Distribution of major periods in IF deposition across geological time, compared against the secular evolution in atmospheric pO_2 levels. Algoma-type IF characterise the mid- to late Archaean and commonly show a temporal connection to submarine volcanic activity, while Rapitan type IF are associated with periods of marine anoxia linked to the Neoproterozoic Snowball Earth. The major peak in volume of IF deposition mentioned in the main text, is represented by the so-called "Lake Superior type" IF from 2.7-2.4 Ga. Also shown is the Mn peak corresponding to the Rhyacian Mn carbonate-black shale associations in west Africa and South America, as well as the timing of the GOE, the Lomagundi carbon isotope excursion (orange bars) and several transient oxygenation episodes (grey arrows; see later text for more details). O_2 curve adapted after Lyons *et al.* (2014).

expense of pre-existing assemblages (Klein, 2005). Unravelling the mineralogy and geochemistry of IF has relied heavily on models and experimental data for diagenetic and metamorphic processes.

In contrast to Fe, sedimentary deposits of Mn show a more widespread temporal distribution during the Proterozoic but were less prevalent prior to this in the Archaean (Roy, 2006; Maynard, 2010; Kuleshov & Maynard, 2016). Many ancient sedimentary Mn deposits exhibit a stratigraphic and sedimentological association with carbonate sequences containing a substantial organic component (black shales; Roy, 2006). The Mn in these rocks is contained almost exclusively in carbonate minerals such as rhodochrosite and kutnohorite, occasionally coexisting with minor Mn silicates (mainly braunite) and very rare sulphide (alabandite; *e.g.*, Mücke *et al.*, 1999). Manganese is present in these minerals predominantly in the 2+ and 3+ oxidation states (Table 1). Overprinting by metamorphism is common and tends to convert the Mn carbonates into largely silicate assemblages, often referred to by the generic term "gondites", with the dominant mineral being the Mn-garnet, spessartine. A characteristic peak in Mn deposits of this kind occurs during the period 2.3-2.0 Ga (Roy, 2006; Fig. 1), as epitomised through the Francevillian in Moanda, Gabon, numerous occurrences in the Birimian of West Africa (*e.g.*, Ghana, Ivory Coast, Burkina Faso, Mali), and deposits of similar age in South America (*e.g.*, Brazil, Guyana). For simplicity, all deposits in this review are termed "Rhyacian Mn deposits" reflecting the geological period when they formed (2300 to 2050 Ma; Fig. 1).

This divergence in the temporal distribution of sedimentary Fe and Mn deposits reveals an apparent first-order decoupling in their aqueous biogeochemistry across the Archaean-Proterozoic boundary (Fig. 1). On the one hand, abundant so-called Superior-type IF of the Neoarchaean-early Palaeoproterozoic (2.7-2.4 Ga) are not associated with marine Mn deposition. Practically all IF-dominated sedimentary sequences of that age (as well as older ones) are impoverished in Mn by comparison to Fe, with only a few occurrences recording weight percent bulk-rock Mn enrichments (Johnson *et al.*, 2013; Kurzweil *et al.*, 2016; Smith et al., 2023). This may reflect the fact that Mn was disseminated more widely, and less likely to be concentrated into localised sedimentary deposits across this period. Furthermore, these Mn enrichments are almost always associated with the carbonate fraction of the rocks, unless secondary (supergene) processes have led to further metal enrichment in the form of residual Mn oxides (*e.g.*, Biwabik IF; Morey *et al.*, 1991). By contrast, while Mn was dominant in Palaeoproterozoic (2.3-2.0 Ga) carbonate-black shale sequences, the concentration of Fe in the same assemblages was comparably muted and restricted chiefly to the pyritic fraction of the carbonaceous hosts.

The transition from intervals dominated first by Fe, then Mn and finally back to Fe-sedimentation corresponds broadly to timescales across the GOE (2.5-1.8 Ga; Fig. 1). At the GOE, a unique sedimentary succession containing both BIF and Mn-rich sedimentary rock was deposited. This is represented by the Hotazel Formation in the Kalahari Manganese Field (KMF) of South Africa. The Hotazel succession records characteristic interlayering between three stratigraphically thick (locally over 50 m), braunite and Mn carbonate-rich sedimentary assemblages, and magnetite/carbonate-rich microbanded facies IF (Tsikos *et al.*, 2003; Fig. 2). The sheer size of the KMF makes it the largest ancient Mn deposit in the geological record, accounting for approximately three quarters of the global land-based reserves of Mn metal (Beukes *et al.*, 2016).

Age constraints for the Hotazel Formation were debated for many years. Recently published U-Pb zircon ages for the Hotazel strata (Schier *et al.*, 2020), baddeleyite U-Pb dates for underlying andesitic volcanic rocks of the Ongeluk Formation (Gumsley *et al.*, 2017) and zircon ages for glacial sediments of the Makganyene Formation (Senger *et al.*, 2023) have provided more clarity. These data can be combined with Pb-Pb ages for carbonates of the overlying Mooidraai Formation (Bau *et al.*, 1999; Fairey *et al.*, 2013) to constrain the age for the Hotazel sequence at *ca* 2.4 Ga. This date supports a close connection with the onset of the GOE, as suggested in previous studies (*e.g.*, Kirshvink *et al.*, 2000) and lies slightly ahead of the loss of mass independent fractionation recorded in multiple S isotopes (Bekker *et al.*, 2004). Early studies suggested that the Hotazel Formation formed in response to the rise in atmospheric oxygen levels through primary Mn^{4+} oxide sedimentation (*e.g.*, Kirshvink *et al.*, 2000; Johnson *et al.*, 2013, 2016). This model is discussed in more detail below.

Table 1. List of key minerals in Fe-rich and Mn-rich sedimentary environments, rocks and their metamorphosed equivalents. Oxidation states are shown for both Fe and Mn; Fe occurs in the 2+ and 3+ redox states, whilst Mn occurs as 2+, 3+ and 4+.

Mineral name	Mineral formula	Group	Oxidation state
Manganite	$Mn^{3+}O(OH)$	Oxyhydroxide	Oxidized
Bixbyite	$(Mn^{3+},Fe^{3+})_2O_3$	Oxide	Oxidized
Hausmannite	$Mn^{2+}Mn_2^{3+}O_4$	Oxide	Mixed
Haematite	$Fe_2^{3+}O_3$	Oxide	Oxidized
Jacobsite	$(Mn^{2+},Fe^{2+},Mg)(Fe^{3+}Mn^{3+})_2O_4$	Oxide	Mixed
Pyrolusite	$Mn^{4+}O_2$	Oxide	Oxidized
Calcite	$CaCO_3$	Carbonate	N/A
Dolomite	$CaMg(CO_3)_2$	Carbonate	N/A
Kutnohorite	$Ca(Mn^{2+},Mg,Fe^{2+})(CO_3)_2$	Carbonate	Reduced
Rhodochrosite	$Mn^{2+}CO_3$	Carbonate	Reduced
Braunite	$Mn^{2+}Mn_6^{3+}SiO_{12}$	Silicate	Mixed
Friedelite	$(Mn^{2+},Fe^{2+})_8Si_6O_{15}(OH,Cl)_{10}$	Silicate	Reduced
Lizardite	$Mg_3Si_2O_5(OH)_4$	Silicate	N/A
Rhodonite	$(Mn^{2+},Fe^{2+},Ca,Mg)SiO_3$	Silicate	Reduced
Ilmenite	$Fe^{2+}TiO_3$	Oxide	Reduced
Magnetite	$Fe^{2+}Fe_2^{3+}O_4$	Oxide	Mixed
Ankerite	$Ca(Fe^{2+},Mg,Mn^{2+})(CO_3)_2$	Carbonate	Reduced
Siderite	$Fe^{2+}CO_3$	Carbonate	Reduced
Chert (quartz)	SiO_2	Silicate	N/A
Greenalite	$(Fe^{2+},Fe^{3+})_{2-3}Si_2O_5(OH)_4$	Silicate	Mixed
Minnesotaite	$(Fe^{2+},Mg)_3Si_4O_{10}(OH)_2$	Silicate	Reduced
Riebeckite	$Na_2[(Fe^{2+},Mg)_3Fe_2^{3+}]Si_8O_{22}(OH)_2$	Silicate	Mixed
Stilpnomelane	$K(Fe^{2+},Mg,Fe^{3+})_8(Si,Al)_{12}(O,OH)_{27}$	Silicate	Mixed
Zircon	$ZrSiO_4$	Silicate	N/A
Arsenopyrite	$Fe^{2+}AsS$	Sulphide	Reduced
Chalcopyrite	$CuFe^{2+}S_2$	Sulphide	Reduced
Pyrite	$Fe^{2+}S_2$	Sulphide	Reduced
Pyrrhotite	$Fe_{1-x}^{2+}S$ (x = 0 to 0.17)	Sulphide	Reduced
Sphalerite	$(Zn,Fe^{2+})S$	Sulphide	Reduced
Apatite	$Ca_5(PO_4)_3(OH,F,Cl)$	Phosphate	N/A
Xenotime	$(Y,HREE)PO_4$	Phosphate	N/A
Monazite	$(Ce,La,Nd,Th)PO_4$	Phosphate	N/A

Fig. 2. Drillcore intersection displaying a typical succession of Fe and Mn-rich subfacies from the base of the stratigraphically upper IF-Mn-IF cycle intersection of the Hotazel Formation in the northern KMF. Younging direction of strata is from left to right: magnetite-carbonate facies microbanded IF (column 1); transitional haematite lutite (columns 2 and 3); laminated and ovoidal carbonate-rich braunitic Mn ore (columns 4, 5 and 6, respectively). Drillcore diameter: 4.5 cm. (Reproduced from Mhlanga *et al.*, 2023).

AIMS AND RATIONALE

As outlined above, the distribution of Fe-rich and Mn-rich sedimentary rocks varies widely across geological time. The mineralogy of these rocks resulted from a combination of primary depositional, diagenetic and metamorphic processes (Table 1). Precursor phases could have been oxyhydroxides, silicates and/or carbonates. Initial sedimentary precipitates would have been subjected to diagenetic and low-grade metamorphic processing with progressive sediment burial (Konhauser *et al.*, 2005, 2007; Walker, 1984). Any subsequent metamorphic processes have added to the overall mineralogical complexity. Interpreting palaeo-depositional redox signals and inferring constraints on global processes is thus challenging.

In this review, formation pathways are put forward to explain the mineralogy of Fe-rich and Mn-rich sedimentary rocks. The mineralogy is then integrated with geochemical data to constrain primary processes in depositional environments. This discussion pays attention to the effects of variable scales of sampling and analysis of the rocks against their intrinsic textural heterogeneity. The potential pitfalls of bulk-rock geochemical interpretations are discussed and possible alternatives, such as sequential chemical extractions, are reviewed. Finally, the record of Fe and Mn deposition is explored before, during and after the GOE, while how this can best inform conceptual models for global oxygenation is also discussed.

RECONSTRUCTING PRECURSOR FE AND MN MINERALOGY

One of the major challenges in the reconstruction of the primary mineralogy of Precambrian IF and Mn-rich sedimentary rocks is the low to non-existent preservation potential of the likely key precursor minerals. This is especially the case with highly reactive oxyhydroxides of Fe and Mn, which typically undergo wholesale reduction either *via* anaerobic diagenesis and/or during the sinking of primary mineral particles through the deeper anoxic waters of redox-stratified basins

(*e.g.*, Konhauser *et al.*, 2005; Johnson *et al.*, 2016; Dreher, 2021; Schad *et al.*, 2022). Consequently, the mineralogy of the Fe and Mn precursors is often inferred from geochemical evidence for redox conditions during their deposition. For example, Mo isotope ratios or Ce anomalies (discussed below) can indicate that conditions were sufficiently oxidizing to generate Mn^{4+}.

Defining the precursor mineralogy depends on models for primary mineral nucleation, which are either (1) conceptually constructed, (2) based on experimental work, and/or (3) built on evidence from modern natural depositional analogues. A concise summary on the current state-of-the-art is presented below starting with Fe precursor minerals, by subdividing the information presented according to the two main schools of thought that have dominated recent research on IF. These can be considered as biological *versus* abiotic formation pathways.

Biological pathways of Fe deposition

Many of the proponents of biologically driven IF deposition (either direct or indirect), have focussed on the role of cyanobacteria in producing oxygen. This free O_2 would be expected to react with dissolved Fe^{2+} under circumneutral pH conditions (*e.g.*, Konhauser *et al.*, 2007) to produce ferric oxyhydroxides such as ferrihydrite [$Fe(OH)_3$]. These minerals could be preserved in the present mineral assemblages of IF as very fine-grained haematite (Sun *et al.*, 2015). The role of cyanobacteria cannot be directly verified in the absence of fossil evidence from the Precambrian sedimentary record, but molecular clock evidence demonstrates that their early evolution was feasible (Soo *et al.*, 2017; Boden *et al.*, 2021).

The main alternative biological pathway that has been suggested in recent years is that of photoautotrophic ferrous iron oxidation under anoxic conditions, widely known as photoferrotrophy (Konhauser *et al.*, 2017; Dreher *et al.*, 2021). Photoferrotrophic bacteria use light to oxidize Fe^{2+} coupled to CO_2 fixation. This results in the precipitation of ferric oxyhydroxide mineral species, predominantly ferrihydrite, and the formation of biomass. As with the cyanobacteria, direct evidence for the role of photoferrotrophes in IF deposition is currently lacking.

Biological precipitation of magnetite is also a potential mineralogical input into precursor IF sediment. One pathway for magnetite authigenesis would be direct precipitation in surface waters mediated by anoxygenic Fe^{2+} photosynthesis (Jiao *et al.*, 2005). However, recent evidence of magnetite formation from two modern ferruginous lakes highlights an alternative depositional pathway. Specifically, Bauer *et al.* (2020) carried out microspectroscopic and geochemical analysis on mineral particles from the water columns and sediments of the ferruginous lakes at Matano and Towuti in Indonesia. Their results show that authigenic magnetite can form as a water-column primary mineral through reduction of biologically precipitated Fe^{3+} phases in anoxic bottom waters. Some of this magnetite takes a characteristic framboidal form that has been interpreted to suggest a possible microbial role during mineral formation. While insights from modern ferruginous lakes are important, they are not perfect analogues for IF deposition. For example, dissolved silica levels are considerably lower in Lake Matano and Towuti than are postulated for Precambrian seawater (Maliva *et al.*, 2005).

Abiotic pathways of Fe deposition

In principle, abiotic models of IF deposition hinge on quantitative interpretations of the ancient rock record, which themselves require an understanding of the rates and processes of Fe mineral precipitation in the early oceans. Over sufficiently long timescales, ferrous mineral precipitation must have been balanced by hydrothermal and continental delivery of Fe^{2+} to the early oceans. Available constraints indicate that dissolved inorganic carbon and $SiO_{2(aq)}$ were abundant in Archaean oceans. Thus, from first principles, mineral sinks that would have controlled Fe^{2+} availability could include Fe^{2+}-silicate precipitation (Rasmussen *et al.*, 2021), Fe^{2+}-carbonate precipitation (Jiang & Tosca, 2019; Jiang *et al.*, 2022), or green rust precipitation (Halevy *et al.*, 2017). Primary Fe^{2+}-hydroxide formation was also recently suggested as an additional abiotic pathway (Dodd *et al.*, 2022).

The pre-GOE sedimentary record abounds with evidence indicating that seawater was persistently anoxic, enriched in silica ($SiO_{2(aq)}$), and at times, ferruginous (Maliva *et al.*, 2005; Planavsky *et al.*, 2011; Poulton & Canfield, 2011; Sperling *et al.*, 2015). In conducting a

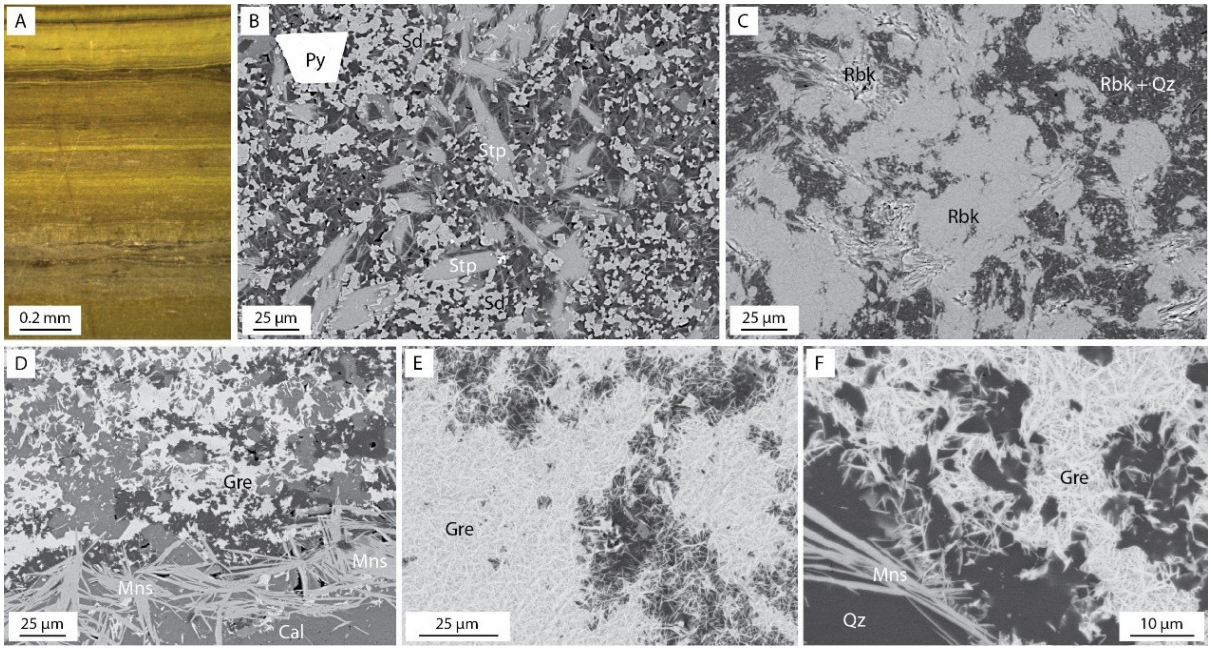

Fig. 3. (A) Thin-section microscope image under plain-polarized light of greenalite-rich microbanded IF from the Kuruman-Griquatown IF transition, Transvaal Supergroup, South Africa. (B-F) Scanning electron microscope images of IF from the Transvaal Supergroup, illustrating common silicate minerals and some of their associations. Mineral abbreviations: Stp: Stilpnomelane; Rbk: Riebeckite; Mns: Minnesotaite; Gre: Greenalite; Cal: Calcite; Sd: Siderite; Py: pyrite; Qz: Quartz. (adapted after Nke *et al.*, 2024).

series of closed-system anoxic precipitation experiments, Tosca *et al.* (2016) observed that over a wide range of conditions relevant to Archaean-Palaeoproterozoic seawater, dissolved Fe^{2+} and $SiO_{2(aq)}$ readily react to precipitate poorly crystalline Fe^{2+}-silicate. This exhibits close structural similarities to the mineral greenalite (Fig. 3), as commonly observed in pre-GOE IF (Rasmussen *et al.*, 2021; Nke *et al.*, 2024). Nucleation of the poorly crystalline Fe^{2+}-silicate precursor directly from the water column could have been triggered by changes in temperature (Tostevin & Ahmed, 2023), pH (Rasmussen *et al.*, 2017; Hinz *et al.*, 2021) or presence of small amounts of Fe^{3+}, followed by structural rearrangement to greenalite.

Green rust, a class of mixed-valence, Fe-rich double layer hydroxides, represents another potentially important mineralization pathway that could have contributed to IF sediments. Based on thermodynamic modelling of a steady-state Precambrian ocean, Halevy *et al.* (2017) suggested that metastable green rust formed in the surface water by partial oxidation (photo-oxidation or by photosynthetic O_2). This could have been a precursor phase which then sank through the water column and decomposed at depth to generate the multiple minerals observed in IF deposits. In investigating this mineralization pathway, Halevy *et al.* (2017) first documented rapid green rust precipitation by exposing anoxic, ferruginous seawater-type solutions to the modern atmosphere for about 1.5 hours. Subsequent ageing of the precipitated green rust in anoxic solutions with various concentrations of dissolved inorganic carbon (DIC) and $SiO_{2(aq)}$ yielded siderite, magnetite, and minor Fe^{2+}-phyllosilicates providing that $SiO_{2(aq)}$ is present. An important advantage of green rust in the context of abiotic mineral formation in IF, is that it does not require organic carbon or microbial processing to produce the mixed valence Fe in many organic-poor IF (compared to the ferric hydroxide $Fe(OH)_3$ pathway discussed earlier; *e.g.*, Konhauser *et al.*, 2005; Sun *et al.*, 2015).

Experimental work on abiotic Fe carbonate growth out of solution (Jiang & Tosca, 2019), indicates that formation of siderite directly from seawater is possible *via* an amorphous Fe carbonate precursor. The latter transforms readily into metastable chukanovite or siderite, dependent on carbonate availability in solution. Precipitation rates estimated from the experiments of Jiang & Tosca (2019) are directly dependent upon the

saturation state of the solution, consistent with theoretical predictions. This relationship, in turn, delineates a critical supersaturation threshold for homogeneous Fe-carbonate precipitation from anoxic and ferruginous water. Subsequent experimental work (Jiang *et al.*, 2022) determined carbon isotope fractionation effects of siderite formation in abiotic seeded growth experiments over a wide range of saturation conditions at 25°C and 1 bar. A key result of this work is that negative carbon isotope values are linked to kinetic isotopic fractionation effects as a function of the degree of solution supersaturation with respect to siderite. They do not thus require an organic carbon source to be accounted for, as has traditionally been postulated for IF carbonate minerals (Dreher *et al.,* 2021). In addition, the range of $\delta^{13}C$ values predicted agrees closely with that of natural siderite and ankerite found in the Precambrian IF record (Tsikos *et al.*, 2022).

Mn precursors

Concerning mineral precursors to Mn formations, the situation is arguably simpler than for IF. Much of the literature on the formation of Mn minerals in anoxic marine basins of the Precambrian, assumes episodically oxic conditions (such as during oxygen oases or "whiffs") in delivering MnO_2 to the primary sediments. However, tetravalent Mn oxide minerals have not been preserved in Mn-enriched IF, nor in black shale-hosted Mn-deposits, and therefore their primary formation is usually inferred through the combined use of redox-sensitive geochemical proxy data (*e.g.*, Mo and Tl isotopes; see Kurzweil *et al.*, 2016; Ostrander *et al.*, 2019). Moreover, abiotic oxidation of Mn^{2+} to Mn^{4+} is very sluggish compared to biological oxidation, which proceeds at rapid rates (Tebo *et al.*, 2004; Namgung *et al.*, 2018). Therefore, the involvement of biology in producing primary Mn^{4+} oxides is typically incorporated into models invoking transient aerobic MnO_2 production before the GOE (Ossa Ossa et al., 2018). Recent work has also suggested an abiotic pathway of Mn^{4+} oxide formation through photooxidation of Mn carbonate under anoxic conditions (Liu *et al.*, 2020).

The possibility that Mn^{3+} species may have been prevalent, both in soluble aqueous form and as solid oxyhydroxide precipitates, has also emerged in the last 20 or so years as a possible alternative to Mn^{4+} (Troubworst *et al.*, 2006; Madison *et al.*, 2013). The observation that Mn^{3+} is a key redox candidate in both sediment porewaters of modern hemipelagic sediments and in the water column of stratified euxinic basins (*i.e.*, Black Sea), takes particular significance in view of experimental studies on abiotic Mn^{2+} oxidation, which indicate that the likely solid mineral products are in fact mixtures of trivalent hydroxides of Mn (mainly MnOOH polymorphs such as feitknechtite) or mixed Mn^{2+} and Mn^{3+} minerals such as hausmannite (Murray *et al.*, 1985; Namgung *et al.*, 2018). Dominance of mixed-valence, Mn^{3+}/Mn^{2+} precursors in anoxic aqueous environments also ties well with the common occurrence of diagenetic minerals of similar valence, such as braunite, hausmannite and/or friedelite, which typify diagenetic to low metamorphic assemblages of many ancient Mn deposits such as those of the KMF (Kleyenstüber, 1984; Nel *et al.*, 1986; Tsikos *et al.*, 2003; Mhlanga *et al.*, 2023).

Finally, recent research has also explored stratified lacustrine environments (*e.g.*, Herndon *et al.*, 2018; Wittkop *et al.*, 2020), in which primary precipitation of Mn^{2+} takes place at the chemocline as Mn carbonate minerals (Mn-calcite, kutnahorite, rhodochrosite). Pathways of primary Mn^{2+} carbonate precipitation have also been supported by the observation of Mn-bearing, high-Mg calcite as a precursor to replacive Fe carbonate in IF, although these environments are not lacustrine (Siahi *et al.*, 2020). These points are revisited below, with particular reference to the *ca* 2.4 Ga Mn deposits of the KMF.

INTEGRATING MINERALOGY WITH GEOCHEMICAL RECORDS

In discussing the origin of IF and Mn deposits and the significance of their mineralogical composition for primary environmental conditions, we must first carefully consider the intrinsic textural heterogeneity typically seen in the rocks. Figure 4 illustrates mineralogical and textural complexity of microbanded IF from South Africa at drillcore (*i.e.*, centimetres to decimetres) scales. It is evident that when selecting a sample for analysis, its size and orientation can lead to a modally and geochemically different composition. This effect is often not taken into sufficient consideration when IF samples are processed as "bulk" materials that combine rock material across successions of mineralogically (and thus compositionally)

distinct bands/laminae.

One way to overcome this potential sampling bias is to target individual bands of IF with specific mineralogical compositions, and treat each of them as a single sample, either through mineral-specific microanalysis (Alibert, 2021; Oonk *et al.*, 2017), or as a bulk material recording a cumulative set of processes and effects. Both options are often cumbersome and impractical undertakings. The rocks are typically very fine-grained on a sub-millimetre to micrometre scale and with complex textural intergrowths (mainly involving Fe silicates; see also Fig. 3), which makes single-grain analysis challenging. Furthermore, bulk-rock analytical approaches to single-band material are hindered by the extremely variable scale of banding combined with compositional heterogeneities within individual bands extending well into the sub-millimetre level (Fig. 5). Contact relationships between bands are thus often diffuse and ill-defined. Bulk rock sampling is only likely to be representative if fine-scale heterogeneities associated with individual bands can be averaged out. The complexities in different scales of laminations in IF make this very challenging.

Application of sequential extraction methodology to IF samples (Oonk *et al.*, 2017, 2018) offers a useful and practical tool through which the geochemistry of the range of minerals in IF can be interrogated. Sequential extraction approaches assume that each mineralogical group is likely to share a similar origin across the sediment column and can therefore be examined individually as a record of distinct processes and conditions of formation through time (Poulton & Canfield, 2005). Optimised extraction protocols have been introduced to target specific geochemical associations that characterise the three key mineralogical fractions of IF, namely the carbonate fraction (siderite, ankerite and lesser calcite), the oxide fraction (chiefly magnetite, with or without haematite), and the silicate fraction (mainly greenalite, stilpnomelane, minnesotaite and riebeckite). Fraction-specific geochemical results for IF are not yet widely available and are currently restricted to the Palaeoproterozoic Kuruman and Griquatown Iron Formations of the Transvaal Supergroup in Griqualand West, South Africa (Oonk *et al.*, 2017, 2018).

The ternary diagram of Fig. 6 summarises average geochemical associations

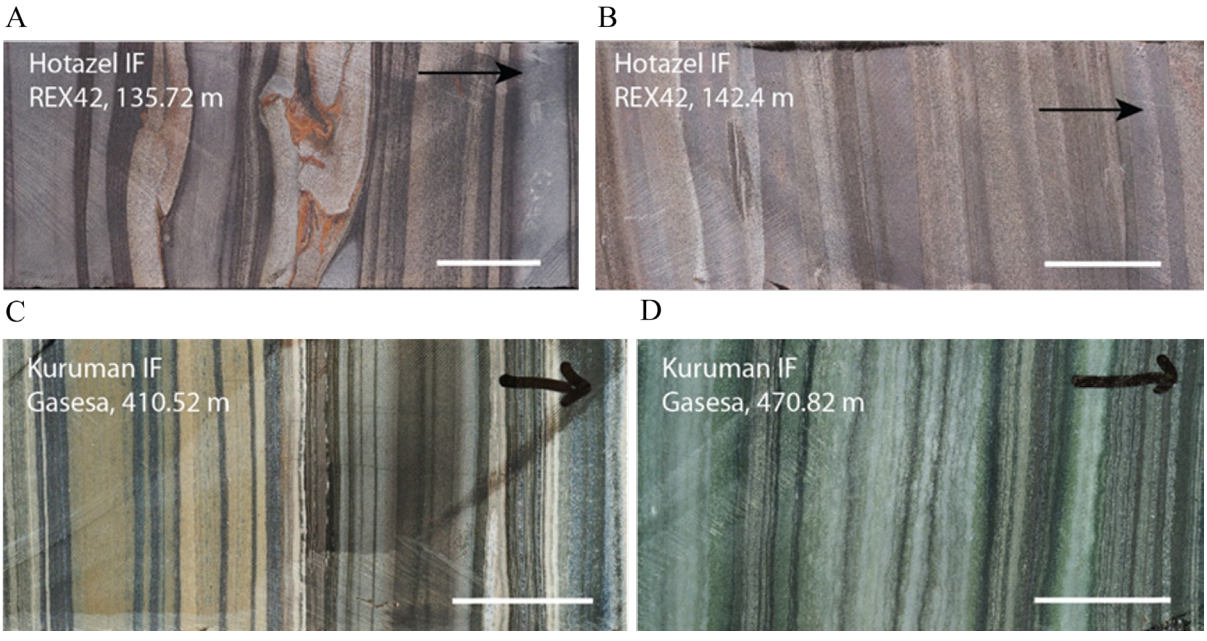

Fig. 4. Microbanded samples from the Hotazel (A, B) and Kuruman (C, D) Iron Formations, Transvaal Supergroup, South Africa, at hand specimen (drillcore) scales. Black arrows illustrate directions of younging, white scale bars are at 1 cm each. Note the heterogeneous composition of the rocks in all cases and on all scales. The Hotazel samples (REX42) illustrate complex compositional banding between chert-carbonate-silicate assemblages (light grey) and magnetite microbands (black). Note also the soft-sediment deformation feature of carbonate-rich chert bands in the top-left sample. The Kuruman samples (GASESA) likewise illustrate complex microbanding between oxide(magnetite)-dominated bands (dark), Fe-carbonate(ankerite+siderite)-dominated chert bands (light grey) and Fe silicate (mainly stilpnomelane)-dominated chert bands (light to dark brown).

that characterise the three main mineral groups in the Kuruman and Griquatown Iron Formations, namely carbonate, oxide and silicate (Oonk *et al.*, 2017). As expected, the element Fe occupies the centre of the diagram due to its broadly equal partitioning across the three mineralogical fractions. Among the other elements that typify IF, Mg is shared almost exclusively between the silicate and carbonate fractions, with minerals such as minnesotaite and ankerite being important hosts. Aluminum dominates the silicate fraction (contained chiefly in stilpnomelane), along with Ti and the two alkali metals Na and K (not shown here). Of particular significance for the discussion that follows is the relationship between Ca and Mn. Both elements show a striking affiliation to the carbonate mineral fraction of IF (Fig. 6), a feature supported by other studies that deal with the origin of Mn enrichments in IF (*e.g.*, Johnson *et al.*, 2013; Kurzweil *et al.*, 2016; Siahi *et al.*, 2020; Smith et al., 2023). Finally, transition metals (*e.g.*, Cu, Ni, V, Co and Cr) show non-unique partitioning among the three mineral groups and are distributed mainly in the lower middle part of the ternary diagram, pointing to their distribution predominantly in the carbonate and silicate mineral fractions.

Fraction-specific geochemical results have provided fresh insights into the nature of the precursor minerals. For example, the results of sequential extractions from the Kuruman and Griquatown Iron Formations suggest that the rare earth element (REE) composition of the Fe carbonate fraction most closely records the seawater REE composition at the time of deposition (Oonk *et al.*, 2018), in a similar fashion to REE data for $CaCO_3$-dominated sedimentary rocks (*e.g.*, Webb & Kamber, 2000). Assuming that pore-water REE patterns were distinct from overlying seawater in BIF-settings, similar to modern siliciclastic and carbonate-dominated settings (Haley *et al.*, 2004), this prompts a reconsideration of carbonate minerals in IF as likely water-column precipitates, or alternatively to be in open contact with the water column through sediment pore fluids during diagenesis. This geochemical similarity to estimated seawater compositions questions the origin of the carbonate as the exclusive product of anoxic diagenesis and organic carbon remineralization deep in the sedimentary pile (Siahi *et al.*, 2020; Tsikos *et al.*, 2022).

At the same time, petrographic and geochemical analysis has demonstrated that IF carbonate records diagenetic recrystallization as well as potential water-column formation (Siahi *et al.*, 2020). Further detailed petrographic and geochemical studies on IF carbonate minerals will be required to fully unlock their potential. Sequential extractions have also been applied to the Mn-rich rocks of the Hotazel Formation with similarly insightful results (Mhlanga *et al.*, 2023). In the sections that follow, reference is made to specific oxide, carbonate, or silicate fractions for IF and Mn-rich rocks from South Africa, with reference to the possible effects of sampling bias where necessary.

IRON FORMATIONS AND MN DEPOSITS PRIOR TO THE GOE

From Fe precursor minerals to IF rock

As outlined above, there are currently two prevailing and contrasting hypotheses for the nature of IF precursors. These place either the minerals ferrihydrite (*e.g.*, Dreher *et al.*, 2021) or greenalite (*e.g.*, Rasmussen *et al.*, 2021) at the centre of the debate. The key difference between these two precursor routes for making IF is that ferrihydrite contains fully oxidized Fe^{3+} whilst greenalite can form from Fe^{2+} as a primary precipitate in anoxic, Si-rich water without the need for oxidation. As discussed previously, deposition of ferrihydrite implicates biological processes as an essential prerequisite for its formation, with primary Fe^{2+} oxidation thought to take place through either anaerobic photoferrotrophy, or *via* oxidation by photosynthetically produced O_2. In contrast, greenalite nucleation could reflect an abiotic depositional setting for primary Fe^{2+} precipitation, although small amounts of Fe^{3+} can be incorporated into the structure (Hinz *et al.*, 2021).

Concerning the oxidation state of Fe in the product IF rocks, the coexistence of ferrous silicates, carbonates, and abundant magnetite in IF results in an intermediate bulk-redox state with an average formal charge of around 2.4-2.5 (Klein, 2005). This means that a ferrihydrite-rich precursor sediment must have undergone substantial Fe^{3+} reduction during diagenesis and burial (*e.g.*, Nims & Johnson, 2022), while a primary greenalite-dominated precipitate would have had to endure at least partial diagenetic disproportionation and/or oxidation to reach the

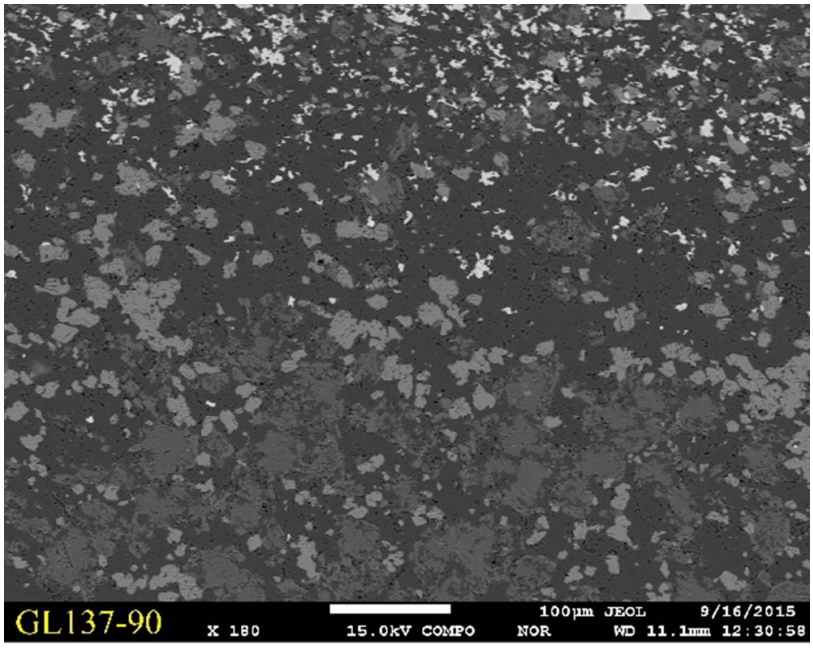

Fig. 5. Back-scattered electron (BSE) image of a chert-carbonate band in the Hotazel IF, illustrating upward gradual variability in mineralogy on sub-millimetre scales. Dark grey grains are ankerite, light grey grains are siderite, bright grains are magnetite, while black background is very fine-grained quartz (chert). (Reproduced from Mhlanga *et al.*, 2023).

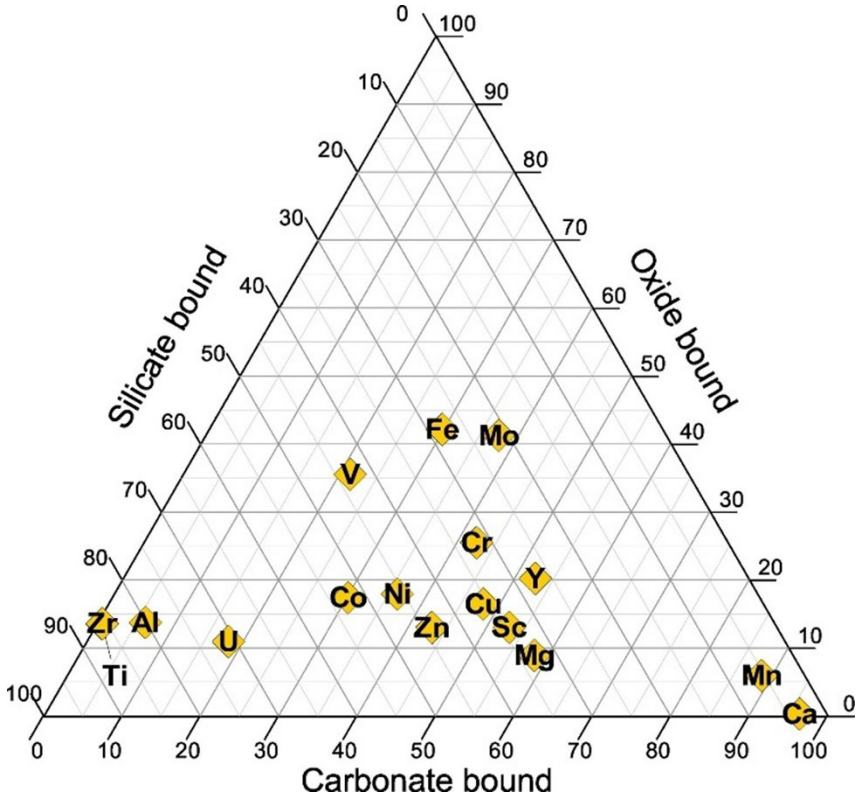

Fig. 6. Ternary diagram illustrating selected major and minor/trace element distributions across the three main mineralogical fractions (silicate, carbonate and oxide) for the Kuruman and Griquatown Iron Formations in the Transvaal Supergroup, South Africa (reproduced from Oonk *et al.*, 2017).

same state (*e.g.*, Rasmussen & Muhling, 2018). In the case of the ferrihydrite pathway, the reductant of choice is biologically derived carbon compounds linked to photoferrotrophy and/or oxygenic photosynthesis, consistent with models of bacterially mediated dissimilatory Fe reduction (DIR) during diagenesis (*e.g.*, Heimann *et al.*, 2010). This is further supported by the formation of low-$\delta^{13}C$ diagenetic Fe carbonates (Dreher *et al.*, 2021). In the case of the greenalite pathway, oxidation has been suggested to occur via oxidising fluids along faults during ore-forming events that post-date the GOE (Rasmussen *et al.*, 2016). It should be noted that a mixed-valence precursor phase such as green rust, would offer a compositionally more plausible alternative than greenalite for the delivery of magnetite and associated Fe carbonate to the diagenetic assemblage of BIF (*e.g.*, Halevy *et al.*, 2017; Chorney & Chemtob, 2022).

Apart from bulk redox considerations for Fe in the system, a key issue is geochemical conservation between precursor sediment and final rock during diagenesis and burial. Neither ferrihydrite nor greenalite can solely account for the bulk mineralogical and geochemical composition of IF as observed today, even if green rust were to be included in the precursor mix. The biggest compositional discrepancy concerns the source(s) of Ca, Mn and Mg in the carbonate fraction of the rocks, a matter which is discussed in more detail in a recent paper by Siahi *et al.* (2020). Here, this is explored further by taking a step back and revisiting the textural heterogeneity of IF as manifested through its characteristic compositional banding across different scales. Sequential extraction work, as outlined in the previous section, has the potential to reveal some important gaps between the presumed precursor mineralogy and the presently observed mineral assemblages.

There are two features of IF that are useful in this discussion: the first is the very close association of Ca and Mn in the carbonate fraction as mentioned in the previous section, and the second is the typical decoupling between the oxide (magnetite) fraction and the carbonate (+silicate) one in discrete layered entities. From the classic viewpoint of compositional banding in IF, although magnetite is present in many mineralogical subfacies as fine-grained disseminations, its predominant mode of occurrence is in the form of typically monomineralic millimetre-scale laminae/bands (Fig. 4). Studies have shown that haematite can be present together with magnetite, but only in some IF and generally in low abundance (Oonk *et al.*, 2017; Konhauser *et al.*, 2017). By contrast, carbonate-rich bands are generally thicker, chert-rich, and often accompanied by various modal abundances of Fe silicate minerals (*e.g.*, minnesotaite, stilpnomelane), with magnetite being a subordinate phase at best. Sequential extraction data for IF (Oonk *et al.*, 2017) show that intervals of maximum Fe precipitation (magnetite-rich layers) are accompanied by minimum contemporaneous Mn precipitation, while intervals of evidently diminished rates of Fe precipitation (carbonate-rich chert bands) record maximum Mn precipitation (relative to Fe). Provided that banding in IF is controlled by – and thus conservatively records – external modulators for periodically variable styles of sediment deposition (*e.g.*, Milankovitch cycles; Lantink *et al.*, 2019, 2023), it follows that deposition must have been controlled by alternation between the manganous and ferruginous zones in a stratified water column.

Let us now consider a situation whereby the precursor Fe species was dominantly ferrihydrite, along with coprecipitated organic carbon and silica (Thompson *et al.*, 2019). Basic mass-balance considerations would suggest that periods of maximum ferrihydrite sequestration accompanied by minimum organic carbon co-precipitation, would conceivably lead to only partial DIR resulting in magnetite-dominated microband formation during diagenesis (*i.e.*, maximum ferric iron preservation). By contrast, comparably lower rates of ferrihydrite deposition along with relatively increased organic carbon and silica precipitation would produce cherty, magnetite-poor, banded ferrous carbonate (+ silicate) assemblages during complete diagenetic DIR (Thompson *et al.*, 2019).

From a geochemical point of view, the additional components required to maintain the mass balance in IF between precursor sediment and rock, are the elements Ca, Mg and Mn that characterise mainly the carbonate(+ silicate) fraction of the relatively Fe-poorer cherty bands. The above leads to a key question regarding redox considerations during IF deposition: what is the primary source for the Mn recorded in the carbonate fraction? The close association between Mn and Ca points to two possibilities

of diverse redox significance, namely Mg calcite together with a Mn^{4+} oxide species produced during transient periods of higher oxidation potential in the environment of deposition; or authigenic, Mn^{2+}-bearing Mg calcite deposited under reducing conditions. Although evidence in favour of the second scenario has already been published (Siahi *et al.*, 2020), the nuances of an interpretation that involves primary Mn^{4+} oxide as the Mn precursor is discussed further below.

Pre-GOE Mn deposition

Episodically high abundances of Mn in IF prior to the GOE have been interpreted as the result of transient bursts of photosynthetic oxygen availability, also termed as oxygen oases or "whiffs" (Anbar *et al.*, 2007; Planavsky *et al.*, 2014; Kurzweil *et al.*, 2016; Ostrander *et al.*, 2019; Robbins et al., 2023). Although such oxygenation events have been alternatively interpreted to represent post-depositional alteration by some authors (*e.g.*, Slotznick *et al.*, 2022), existing models are supported by Mo and Tl isotope studies (Kurzweil *et al.*, 2016; Ostrander *et al.*, 2019, 2024), whereby isotope fractionation of both metals can be explained by adsorption onto primary Mn^{4+} oxide precipitates. Preservation of the primary isotopic signals during diagenesis and burial of Mn^{4+} oxides is a prerequisite in this interpretation. However, to date, no Mn^{4+} or Mn^{3+} oxides have been found to be preserved in Mn-enriched IF. This might be explained by loss of the oxides through quantitative reductive recycling of Mn^{4+} as Mn^{2+} into diagenetic Fe carbonate minerals (*i.e.*, siderite and ankerite). At the same time, organic carbon preservation as the essential reductant of the primary Mn^{4+} oxides in this model, is also scarce or absent in IF, including those that are Mn-enriched (Dodd *et al.*, 2019; Tsikos *et al.*, 2022). The lack of organic carbon could be explained if there were an abundance of electron acceptors (*e.g.*, Fe^{3+} minerals) in such a depositional system.

Bulk Mn/Fe ratios of IF have been used as a redox proxy to assess this further. A recent study (Wang *et al.*, 2022) explores an apparent secular change in the bulk Mn/Fe ratio of IF in line with the basic premise of transient oxygenation models. The temporal rise in the Mn/Fe ratio of IF from the Archaean to the Palaeoproterozoic is interpreted to correspond to progressively more oxidative conditions, associated with higher rates of precursor Mn^{4+} oxide deposition in the primary IF sediment. Rising Mn/Fe ratios in IF are coupled with a corresponding decline in bulk Fe isotope values, the latter interpreted to record a combination of long-term reservoir effects on the $\delta^{56}Fe$ of the oceanic $Fe^{2+}_{(aq)}$ inventory (for a comprehensive review of Fe isotopes in IF, see Johnson *et al.*, 2008). These effects would include predominantly partial Fe^{2+} oxidation during deposition in the Archaean leading to highest $\delta^{56}Fe$ values recorded in IF, followed by more quantitative oxidation and precipitation of the progressively ^{56}Fe-depleted $Fe^{2+}_{(aq)}$ inventory by the earliest Palaeoproterozoic. The strength of this model hinges on the premise already outlined above that primary ferrihydrite (+ Mn^{4+} oxide) precipitation, and its initial isotopic composition through time, were preserved in the rocks under essentially closed system conditions of diagenetic Fe (and Mn, where relevant) reduction and associated mineral formation.

Alternative interpretations for this apparent secular redox trend in IF must bring into consideration the textural and compositional heterogeneity of the rocks, together with geochemical mass balance constraints and the demonstrated strong partitioning of Mn into the carbonate fraction. Sequential extraction results suggest that the bulk Mn/Fe ratio in IF corresponds effectively to the bulk carbonate/oxide ratio of the rock (Oonk *et al.*, 2017). Diagenetic Fe carbonate formation is known to be accompanied by strong fractionation of the light Fe isotope into ferrous carbonates (Johnson *et al.*, 2008). This would presumably leave behind residual unreacted oxide (likely as magnetite) that would have to be further enriched in the heavy Fe isotopes than the precursor ferrihydrite to satisfy conservative preservation of the bulk $\delta^{56}Fe$ signal. Similar fractionation effects would also be expected *via* formation of diagenetic ferrous silicate(s) (*e.g.*, greenalite) against the same oxide precursor(s). The degree of Fe isotope fractionation between reactant ferric oxide and resultant Fe carbonate (+ silicate), would thus be broadly commensurate with the relative modal abundance of these phases in the final mineral assemblage. It follows that only in the case of fully quantitative closed-system reduction of the ferric oxide to form carbonate or silicate, would the bulk $\delta^{56}Fe$ signal remain unchanged.

If the above assumptions hold true, then the way in which heterogenous IF is sampled for

chemical and isotopic analyses becomes crucial for reliable interpretations relevant to redox evolution. For example, selection of an oxide-dominated (*e.g.*, magnetite-rich) sample from a hand specimen or drill core section should return a δ^{56}Fe value that is more positive than that of an adjacent sample that is relatively more siderite-rich and/or greenalite-rich. Similarly, an oxide-rich sample would have a substantially lower Mn/Fe ratio than a siderite(+greenalite)-rich one, based on the fraction-specific geochemical relationships explained above. A series of questions naturally follow these considerations: first, what can be reasonably defined as a geochemically closed system in an IF in terms of diagenetic mineral formation and isotopic exchange between the precursor (reactant) and the diagenetic (product) minerals? What exact criteria would dictate the extent of a closed system in an IF sample? Would it be a single band of any composition? A single couplet of a magnetite-rich band adjacent to a chert-carbonate(±silicate) one? Or a bundle of such couplets sharing closely similar mineralogical and mineral-chemical attributes? Furthermore, is it reasonable to assume that mineralogically distinct bands must always record predictable chemical and isotopic signatures and physicochemical conditions of primary ferrihydrite nucleation through time? If so, must this apply universally, irrespective of the large modal and/or qualitative mineralogical variability typically observed in IF assemblages from one band to the next?

Pathways with alternative precursor minerals

Focus on ferrihydrite or greenalite as the main precursor species during IF deposition may not fully address the compositional characteristics of the carbonate or silicate fractions. Recent literature supports sequestration of Mn-rich carbonate minerals in the precursor sediment of redox-stratified lakes and in IF as primary water-column precipitates (Herndon *et al.*, 2018; Jiang & Tosca, 2019; Wittkop *et al.*, 2020; Siahi *et al.*, 2020). Suggestions have also been made for a large fraction of IF carbonates to have been derived from the ambient water column as primary precipitates, thus accounting for the dearth of organic carbon preservation in IF (Thompson *et al.*, 2019). Furthermore, although primary carbonates forming in modern stratified lakes obtain their low δ^{13}C signatures largely from methane or organic matter oxidation in the water column (*e.g.*, Havig *et al.*, 2017), non-equilibrium carbon-isotope fractionation processes may alternatively account for the low δ^{13}C signatures as recorded in IF carbonates (Jiang *et al.*, 2022). This would remove the need to invoke organic carbon remineralization in carbonate formation, although evidence for kinetic isotopic fractionation has not yet been independently observed in marine Mn-rich carbonates. The same isotopic fractionation processes also provide additional explanation for the paucity of organic carbon preservation in IF in general (Dodd *et al.*, 2019). Finally and more crucially, as elevated Mn contents in IF carbonates are likely to record carbonate saturation in equilibrium with $Mn^{2+}_{(aq)}$-enriched waters similar to their modern lacustrine counterparts, primary Mn-rich carbonate formation does not have to be accounted for exclusively through aqueous Mn^{2+} oxidation to Mn^{4+} first, only to be succeeded by quantitative diagenetic reduction back to Mn^{2+} and its incorporation into carbonate minerals (Johnson *et al.*, 2016).

Models involving Fe silicates as the alternative precursor to IF are also not short of complications. Primary greenalite formation may involve not only mechanisms of authigenic nucleation directly from an anoxic Fe^{2+}-rich pool but can also be linked to reductive shuttling of biogenically (or abiotically) nucleated ferric hydroxides through adsorption onto silicates in the primary anoxic water column (*e.g.*, Fischer & Knoll, 2009; Schad *et al.*, 2022). This could be tested using Fe isotope compositions of greenalite which ought to result in substantially different Fe isotope signatures for each of the above pathways. Furthermore, the silicate minerals stilpnomelane and minnesotaite are compositionally distinct from greenalite, are commonly present in close paragenetic association with carbonate minerals and may themselves record specific processes of primary formation together with the carbonates (Fig. 7).

Finally, the sodic silicate mineral riebeckite is omnipresent in many South African and Australian IF successions, including the Mn-rich Koegas IF in the Transvaal Supergroup (Kurzweil *et al.*, 2016). It often exhibits textures indicating formation at the latest during early diagenesis (*e.g.*, Fairey *et al.*, 2013). Previous work has suggested that the source of the Na was metasomatic (Miyano & Beukes, 1997), but riebeckite nucleation in IF does not necessarily

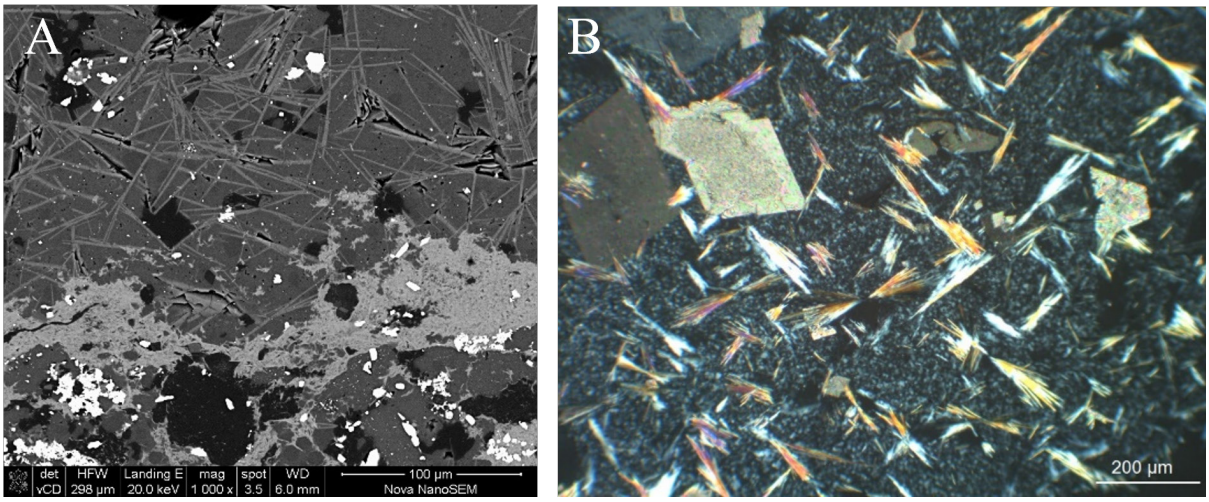

Fig. 7. A: Back-scattered electron (BSE) image from a calcite-rich band in the Hotazel IF (dark grey, top of image) in textural association with dispersed stilpnomelane needles (light grey). Lighter grey micro-crystalline mass below represents fine-grained minnesotaite, bright grains are magnetite, while black background is chert. B: Petrographic view under cross-polarized light of a typical association of disseminated acicular minnesotaite and rhombohedral ankerite in a chert microband from the Griquatown IF.

require a universally exotic source of Na for its formation. Despite the many textural diagenetic effects likely to be involved in the formation of mineral assemblages in IF, it is entirely possible that every mineralogically discrete band originates from a combination of specific primary processes and conditions in a temporally dynamic depositional environment, and therefore deserves to be treated as a distinct subsystem and faithful record of these processes.

THE HOTAZEL IF-MN FORMATION AND THE POST-GOE MN SPIKE

The exact timing and extent of oxygenation across the GOE has been extensively debated. Attempts to constrain the timing of first oxidation of $Mn^{2+}_{(aq)}$ to insoluble Mn^{4+} oxides have produced conflicting results. On the one hand, proponents of transient oxygenation events (*i.e.*, O_2 oases and "whiffs") propose that oxidation of Mn^{2+} to Mn^{4+} would have occurred well before the GOE, supported by Mo and Tl isotope evidence (*e.g.*, Anbar *et al.*, 2007; Kurzweil *et al.*, 2016; Ostrander *et al.*, 2019). Studies specifically targeting Mn-enriched IF, invoke processes of Mn^{2+} to Mn^{4+} oxidation to have taken place as far back as the Mesoarchaean (Planavsky *et al.*, 2014; Robbins et al., 2023; Smith *et al.*, 2023), thus supporting the onset of oxygenic photosynthesis and development of localised oxygen oases already by that time (*e.g.*, Riding *et al.*, 2014; Wilmeth *et al.*, 2019).

However, as already mentioned above, Mn^{4+} is not preserved in the sedimentary record and evidence in support of such models is primarily isotopic (*e.g.*, Planavsky *et al.*, 2014; Wang *et al.*, 2018; Ossa Ossa *et al.*, 2018, 2019; Hiebert et al., 2018). This isotopic evidence has been brought into question and alternatively linked to post-depositional hydrothermal effects in some cases (Slotznick *et al.*, 2022). It is possible to draw from this that the development of transiently oxic conditions before the GOE, capable of driving full oxidation of Mn^{2+} to its tetravalent state, is a notion that is not unequivocal.

In this light, the IF and Mn deposits of the Hotazel Formation potentially provide insights to the ongoing debates. The origin of the Hotazel Formation was recently reviewed and reinterpreted through a comprehensive new dataset of fraction-specific geochemical results and stable isotope data (C, Fe), collected at high stratigraphic resolution (Mhlanga *et al.*, 2023). The results of the work by Mhlanga *et al.* (2023) that are of direct relevance to this discussion are summarised here.

The Hotazel Formation is a unique interlayered succession of microbanded IF and three layers of Mn-rich sedimentary rock (Fig. 2). The most striking geochemical characteristic of the Hotazel succession is the strong separation between two first-order sedimentary facies with respect to Mn concentration (Fig. 8). On the one hand, the Hotazel IF records bulk average

concentrations of Mn (as MnO) around 0.5 wt%, while the three Mn-rich sedimentary layers have bulk MnO contents ranging from 25 wt% to over 40 wt%. Respective bulk Fe_2O_3 concentrations in the IF have average values generally between 35 and 50 wt%, while in the interbedded Mn layers they range from less than 10 wt% to as high as 25 wt%.

The mineralogy of the Hotazel IF and Mn-rich strata provides additional insights with respect to the primary conditions and processes of Mn mineral formation and deposition. As expected, the very low amounts of Mn in the Hotazel IF are contained exclusively in the carbonate fraction of the rocks, which is typified by the assemblage of ankerite and siderite with the addition of appreciable calcite (Fig. 7). In other words, the carbonate fraction of the IF is typically Fe-rich, but still accounts for the small amounts of Mn contained in bulk rock. In terms of Fe, the Hotazel IF is haematite-poor and magnetite-rich, except for its lowermost stratigraphic portion that is Mn-bearing and contains abundant haematite and carbonate, and thus appears compositionally transitional to Mn-rich facies (Lantink *et al.*, 2018).

In stark contrast to the IF, the Hotazel Mn-rich layers contain haematite as the sole Fe oxide mineral while their carbonate mineralogy is exclusively Mn-rich and Fe-poor. Curiously, the Mn content in the carbonate fraction of these rocks is highest in the haematite-rich lithological transitions that typically characterise the contacts between IF and Mn layers (so-called "haematite lutite" zones; Fig. 2) and have low bulk-rock Mn values. This Mn enrichment in the carbonate drops off substantially as maximum bulk-rock Mn concentrations are reached (Fig. 8). High bulk-rock Mn contents are accounted for by peak modal abundances of the mineral braunite, in concert with diminishing Mn contents in co-occurring carbonate. In all instances, however, the Fe content of the carbonate fraction remains vanishingly low. In summary, the bulk carbonate mineral fraction across the entire Hotazel Formation records spectacular fractionation between Fe-rich/Mn-poor and Mn-rich/Fe-poor mineralogy, which respectively characterises the corresponding IF and Mn-rich sedimentary hosts.

Constraining the precursor Mn species in the Hotazel Formation rocks is crucial to palaeoenvironmental reconstructions and has consequently been the subject of much research and debate. The first model to consider is that of precipitation of primary Mn^{4+} oxide that was subsequently respired into low-$\delta^{13}C$ Mn carbonates and braunite upon reduction by organic matter during microbially mediated anaerobic diagenesis (Johnson *et al.*, 2016). Reduction of Mn^{4+} must have been quantitative, given the lack of preservation of any Mn^{4+}-containing minerals. At the same time, organic carbon contents in the Hotazel Mn layers are also essentially undetectable, while there is no mineralogical evidence for any Fe^{3+} reduction to Fe^{2+}.

In their recent paper, Mhlanga *et al.* (2023) refute the need for massive primary MnO_2 precipitation leading to the formation of the Hotazel Mn strata through reductive diagenetic pathways. Their arguments centre around their carbonate-specific results, which record minimum Mn^{2+} uptake in the carbonate fraction of the rocks simultaneously with maximum rates of braunite (*i.e.*, Mn^{3+}) deposition. The diagenetic model of Mn carbonate formation in the Hotazel rocks, seems to fall short in terms of addressing the occurrence of low-Mn calcic carbonates during periods of maximum Mn availability in the sediment, as the exact opposite is predicted to occur. Primary pathways of carbonate formation are therefore proposed as viable alternatives, with the low-$\delta^{13}C$ carbonate signatures explained possibly *via* non-equlibrium isotopic effects in exchange with ambient seawater DIC, in a similar fashion to experimental Fe carbonate formation (Jiang *et al.*, 2022).

The abundance of braunite in the Hotazel Mn assemblages in combination with published experimental results of inorganic Mn^{2+} oxidation (Murray *et al.*, 1985; Namgung *et al.*, 2018), lend support to the possibility that the precursor Mn mineral may have been a Mn^{3+} oxyhydroxide (MnOOH) instead of MnO_2. Primary, Mn-bearing calcic carbonate and MnOOH precipitation are thus interpreted to have taken place during periods of maximum regression in a dynamic and delicately poised stratified marine basin with respect to both Fe and Mn redox cycling (Fig. 9). This would implicate Mn^{3+} as key electron acceptor, possibly for the first time in Earth history (Trouwborst *et al.*, 2006; Madison *et al.*, 2013).

Braunite formation could have ensued through reaction of precursor MnOOH-rich sediment with pore-fluids containing dissolved silica and Mn^{2+} (Koshurba & Johnson, 2024). In

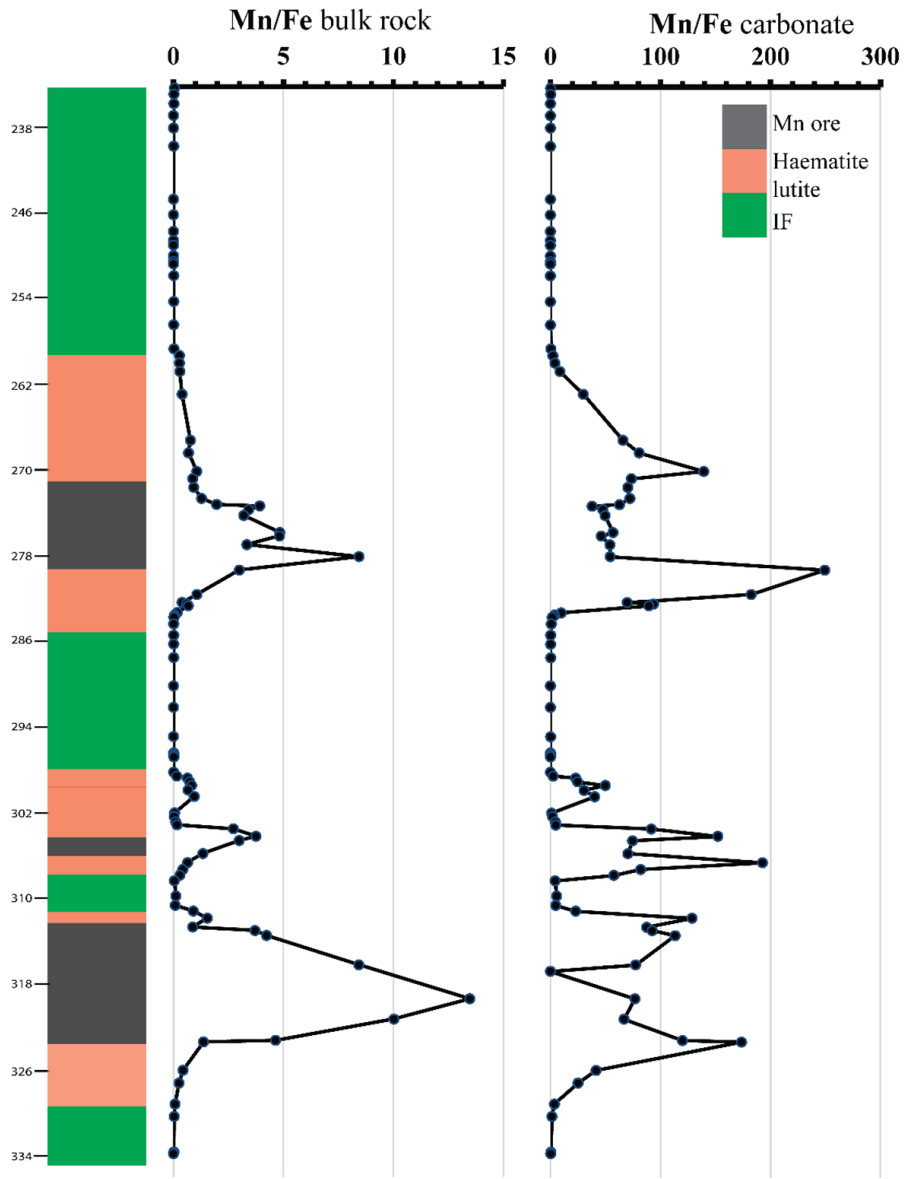

Fig. 8. High-resolution chemostratigraphic profiles of bulk and carbonate-specific Mn/Fe ratios across the entire Hotazel Formation from Gloria mine, northern KMF. Note the sharp decline in carbonate-specific Mn/Fe ratios at the level of maximum bulk-rock ones, displayed most eloquently in the upper IF-Mn-IF cycle (modified after Mhlanga *et al.*, 2023). Vertical scale in metres below present surface.

this light, it is thought that the KMF depositional environment and its sedimentary products must have characterised only the period leading up to the onset of the GOE. The latter argument is founded primarily on the preponderance of braunite as a stable diagenetic Mn^{3+} mineral in an apparently impoverished primary sediment with respect to Si, given that no free quartz is documented from the KMF Mn ores (Miyano & Beukes, 1987; Tsikos *et al.*, 2003). Classic IF, by contrast, are highly siliceous rocks with bulk SiO_2 content around 50 wt% or higher. It is difficult to explain why older, Mn-enriched IF with typically high SiO_2 concentrations are not reported to contain Si-bearing Mn minerals such as braunite, while the postulated Mn^{4+} precursors are thought to be quantitatively reduced to diagenetic Mn carbonates, and organic carbon as the reductant of choice is never preserved in the rocks.

In terms of Mn redox, records of REE geochemistry provide important additional constraints. The oxidation of Ce^{3+} to Ce^{4+} in oxic waters commonly occurs on the surface of Mn^{4+} oxide particles. As a result, the redox chemistry of

Ce and Mn are closely linked (*e.g.*, Nakada et al., 2016). These processes result in enrichments in Ce in Mn^{4+} oxide minerals ("positive anomalies") as well as depletions in Ce in the surrounding seawater ("negative anomalies"). The seawater signal should be faithfully recorded by the carbonate phase (Webb & Kamber, 2000; Tostevin et al. 2016), as well as rapidly precipitated Mn and Fe oxide minerals (Koschinsky *et al.*, 1996). It follows that massive deposits of Mn^{4+} oxides in the rock record would have similar potential to record Ce anomalies in their REE patterns, provided that they were deposited under sufficiently oxidizing bottom and shallow pore-water conditions to preserve Mn^{4+} minerals. However, positive and negative Ce anomalies are largely absent from both the Mn-rich layers and host IF in the Hotazel Formation, although a small number of examples have been reported (Schier *et al.*, 2020). They therefore compare very well with REE patterns from classic pre-GOE IF (Planavsky *et al.*, 2010), which are largely devoid of Ce anomalies. Such signals thus provide little support for massive marine Mn^{4+} deposition and attendant Ce fractionation during deposition of the Hotazel Formation.

Indirect geochemical evidence for the occurrence of Mn^{4+} oxides in the marine realm of the Proterozoic can be found in the Rhyacian Mn deposits of west Africa and analogous occurrences

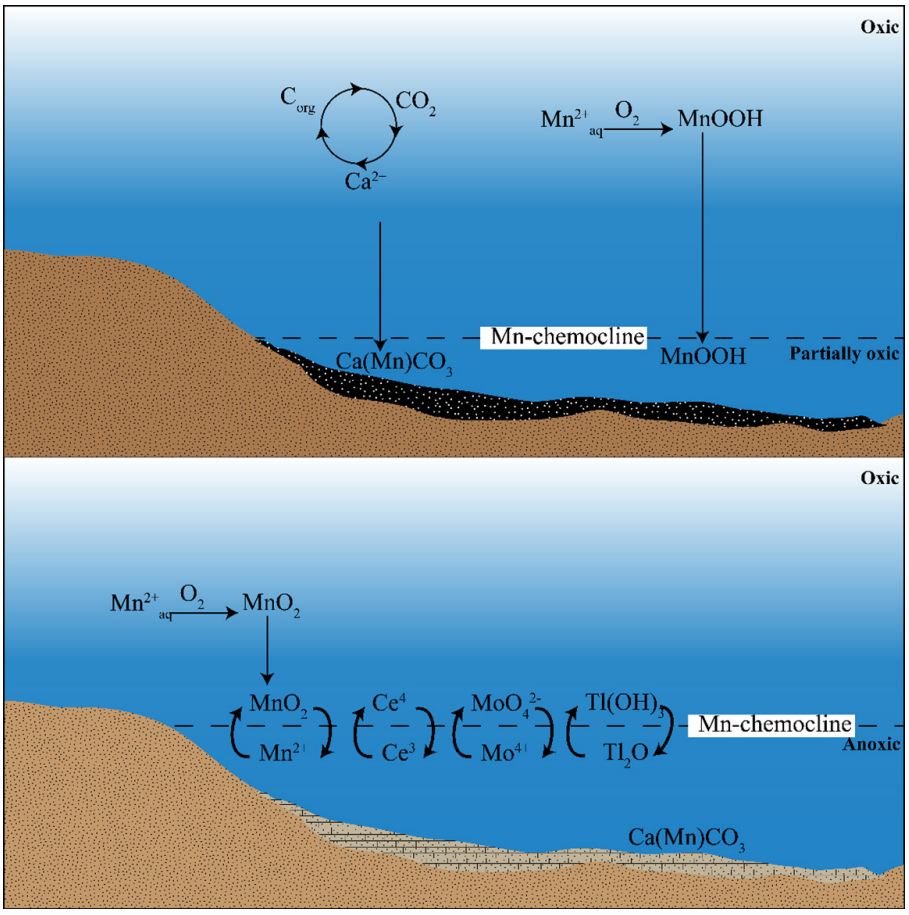

Fig. 9. Simplified view of a redox-stratified basin characterised by a Mn shuttle mechanism and Mn deposition in the period leading up to the GOE (top) and during post GOE times (bottom). In the pre-GOE case (after Mhlanga *et al.*, 2023), the model assumes aerobic oxidation of Mn^{2+} to Mn^{3+} and deposition of Mn predominantly as MnOOH, later converted to braunite diagenetically. Carbonate deposition here is restricted to relatively low Mn calcite and kutnahorite. In the post-GOE case (after dos Santos *et al.*, 2022), converted oxides derived from Mn^{2+} oxidation in oxic surface waters, are reductively recycled at the Mn-chemocline. Along with Mn, redox-sensitive trace elements such as Ce, Mo and Tl are also oxidized and subsequently reduced at the chemocline. Resultant Mn carbonate saturation and nucleation below the chemocline, records and transfers the trace element signals from the anoxic water reservoir into the Mn carbonate-rich sediment at the seafloor. This model can explain the redox signatures as preserved at least in Rhyacian Mn carbonate deposits such as the Borborema deposit of Brazil.

in South America (see also Fig. 1). At least two case studies from Brazil report positive Ce anomalies in Mn carbonate mineralization. In the case of the Sierra do Navio deposit (Chisonga *et al.*, 2012), the Ce anomalies are interpreted to be derived from recycling of primary Mn^{4+} oxides during anaerobic diagenesis involving organic matter, and preservation of the positive Ce anomalies in the low-$\delta^{13}C$ Mn carbonate ores through late diagenesis and subsequent metamorphism. In the Borborema deposit, however, similar anomalies are interpreted through water-column Mn carbonate nucleation following an active Mn^{4+} oxide shuttle (dos Santos *et al.*, 2022; Fig. 9). Here, preservation of the positive Ce signal is thought to have taken place in anoxic bottom waters below a chemocline, and not through reductive Mn^{4+} oxide reworking strictly during organic matter diagenesis below the sediment-water interface. Whatever the exact pathway, positive Ce anomalies at both sites appear to offer support to sufficiently oxic oceanic conditions being attained by approximately 2.3 Ga, to drive Mn^{2+} oxidation fully to its tetravalent state. Additional support to this model is seen in the Mo isotope record of the Nsuta deposit in Ghana (Goto *et al.*, 2021) and the Morro da Mina deposit in Brazil (Cabral *et al.*, 2019), in the latter case with positive Ce anomalies being preserved through a high-grade metamorphic overprint.

CONCLUSIONS

Precambrian sedimentary rocks enriched in Fe and Mn have been the target of ongoing and intensive research and have generated an immense body of knowledge on the coevolution of oxygen and life on Earth. The advent of new and increasingly powerful geochemical tools has accelerated our knowledge of ancient marine and terrestrial surface environments and the emergence of coupled biogeochemical cycles. This review highlights the numerous biologically mediated and abiotic pathways that have been proposed for precursor Fe and Mn mineral deposition.

Iron formations and manganese deposits are petrologically challenging to study, with mineral assemblages that reflect a combination of processes from the primary depositional environment, through diagenesis and metamorphism to the final rock outcrop or drill core. The way in which the rocks are sampled, and the scale on which geochemical information is obtained, means that interpretations are subject to the inherent heterogeneity of banding on multiple scales. This can have a strong influence on resulting conceptual models for redox conditions and the role of biological processes in the original sedimentary environment. Sequential extraction protocols offer a new perspective to tackle this heterogeneity by independently targeting carbonate, oxide and silicate mineral fractions. Initial results show that widely accepted models for Fe and Mn deposition invoking primary precipitates as ferrihydrite and Mn^{4+} oxides, coupled with diagenetic reworking of buried organic matter, may need to be revisited.

In this review, specific examples are shown of volumetrically large accumulations of Fe-rich and Mn-rich sediments deposited before, during and after the first major accumulation of free oxygen in the Earth's atmosphere, the so-called Great Oxidation Event. Iron and Mn deposition are decoupled from one another and do not show a direct relationship to atmospheric oxygenation. Preliminary evidence suggests a transition from a system where Mn was processed predominantly through the Mn^{2+} and Mn^{3+} oxidation states at the start of the GOE, to one where oxidation proceeded to produce Mn^{4+} by the Rhyacian Period at its end. Despite the complexities of interpreting these rocks, it is possible to conclude that their mineralogy and abundance do reflect major redox changes in the primary depositional environment.

ACKNOWLEDGEMENTS

HT and XM acknowledge generous support from ASSMANG Ltd, and particularly Mrs. C. van der Merwe, Mr. B. Ruziwe, Mr M. Burger (retired) and Mr. I van Niekerk, for their long-standing commitment to the PRIMOR research unit that operated at Rhodes University during the period 2014-23. RT and AN wish to thank the NRF BIOGRIP platform and NRF-COEs Genus and CIMERA. Special thanks are also extended to the geological staff of SOUTH32 in Hotazel, especially Mr. T. Rambuda and Mr. E.P. Ferreira (retired), for their open-door policy and unconstrained access to their drill core facility for the purposes of our research.

REFERENCES

Alibert, C. (2021) Rare earth elements in Hamersley BIF minerals. *Geochim. Cosmochim. Acta*, **184**, 311−328.

Anbar, A.D., Duan, Y., Lyons, T.W., Arnold, G.L., Kendall, B., Creaser, R.A., Kaufman, A.J., Gordon, G.W., Scott, C., Garvin, J. and **Buick, R.** (2007) A whiff of oxygen before the great oxidation event? *Science*, **317**, 1903−1906.

Bau, M., Romer, R.L., Lüders, V. and **Beukes, N.J.** (1999) Pb, O, and C isotopes in silicified Mooidraai dolomite (Transvaal Supergroup, South Africa): Implications for the composition of Paleoproterozoic seawater and 'dating' the increase of oxygen in the Precambrian atmosphere. *Earth Planet. Sci. Lett.,* **174**, 43−57.

Bauer, K.W., Byrne, J.M., Kenward, P., Simister, R.L., Michiels, C.C., Friese, A., Vuillemin, A., Henny, C., Nomosatryo, S., Kallmeyer, J., Kappler, A., Smit, M.A., Francois, R. and **Crowe, S.A.** (2020) Magnetite biomineralization in ferruginous waters and early Earth evolution. *Earth Planet. Sci. Lett.,* **549**, 116495.

Bekker, A., Holland, H.D., Wang, P-L., Rumble 3rd, D., Stein, H.J., Hannah, J.L., Coetzee, L.L. and **Beukes, N.J.** (2004) Dating the rise of atmospheric oxygen. *Nature*, **427**, 117−20.

Bekker, A., Slack, J.F., Planavsky, N., Krapez, B., Hofmann, A., Konhauser, K.O. and **Rouxel, O.J.** (2010) Iron formation: the sedimentary product of a complex interplay among mantle, tectonic, oceanic, and biospheric processes. *Econ. Geol.*, **105**, 467−508.

Bekker, A., Planavsky, N.J., Krapež, B., Rasmussen, B., Hofmann, A., Slack, J.F., Rouxel, O.J. and **Konhauser, K.O.** (2013) Iron Formations: Their Origins and Implications for Ancient Seawater Chemistry. *Treatise. Geochem: Second Edition.,* **9**, 561−628.

Bekker, A. and **Kovalick, A.** (2021) Ironstones and iron formations. Alderton D., Elias S. A. (eds.). Encyclopedia of Geology (2nd ed.). *Oxford: Academic Press*, 914−921.

Beukes, N.J. (1983) Palaeoenvironmental setting of iron-formations in the depositional basin of the Transvaal Supergroup, South Africa. *Dev. Precambrian. Geol.*, **6**, 131−142.

Beukes, N.J., Swindell, E.P.W. and **Wabo, H.** (2016) Manganese Deposits of Africa. *Episodes,* **39**, 285−317.

Boden, J.S., Konhauser, K.O., Robbins, L.J. and **Sánchez-Baracaldo, P.** (2021). Timing the evolution of antioxidant enzymes in cyanobacteria. *Nat. Commun.*, **12**, 4742.

Cabral, A.R., Zeh, A., Vianna, N.C., Ackerman, L., Pašava, J., Lehmann, B. and **Chrastný, V.** (2019) Molybdenum-isotope signals and cerium anomalies in Palaeoproterozoic manganese ore survive high-grade metamorphism. *Sci. Rep.,* **9**, 4570.

Canfield, D.E., Kristensen, E. and **Thamdrup, B.** (2005) The Iron and Manganese Cycles. *Adv. Mar. Biol.,* **48**, 269−312.

Chisonga, B.C., Gutzmer, J., Beukes, N.J. and **Huizenga, J.M.** (2012) Nature and origin of the protolith succession to the Paleoproterozoic Serra do Navio manganese deposit, Amapa Province, Brazil. *Ore Geol. Rev.*, **47**, 59−76.

Chorney, A.P. and **Chemtob, S.M.** (2022) Iron precipitation under controlled oxygen flow: Mineralogical implications for BIF precursors in the Archean ocean. *Chem. Geol.,* **618**, 121279.

Dodd, M.S., Wang, H., Li, C., Towner, M., Thomson, A.R., Slack, J.F., Wan, Y.-S., Pirajno, F., Manikyamba, C., Wang, Q. and **Papineau, D.** (2022) Abiotic anoxic iron oxidation, formation of Archean banded iron formations, and the oxidation of early Earth. *Earth Planet. Sci. Lett.,* **584**, 117469.

Dodd, M.S., Papineau, D., Pirajno, F., Wan, Y. and **Karhu, J.A.** (2019) Minimal biomass deposition in banded iron formations inferred from organic matter and clay relationships. *Nat. Commun.*, **10**, 1−13.

dos Santos, F.H., da Silva Amaral, W., Chi-Fru, E., de Souza, A.C.B. and **Bosco-Santos, A.** (2022) Paleoproterozoic manganese oxide precipitation in oxic seawater surface and reductive enrichment in anoxic seafloor. *Chem. Geol.*, **588**, 120655.

Dreher, C.L., Schad, M., Robbins, L.J. Konhauser, K.O., Kappler, A. and **Joshi, P.** (2021) Microbial processes during deposition and diagenesis of Banded Iron Formations. *Palaontol. Z.*, **95**, 593-610.

Fairey, B., Tsikos, H., Corfu, F. and **Polteau, S.** (2013) U–Pb systematics of the Postmasburg Group, Transvaal Supergroup, South Africa: Primary versus metasomatic controls.

Precambrian Res., **231**, 194−205.

Fischer W.W. and **Knoll A.H.** (2009) An iron shuttle for deepwater silica in late Archean and early Paleoproterozoic iron formation. Geol. Soc. Am. Bull., **121**, 222–235.

Fischer, W.W., Hemp, J. and **Johnson, J.E.** (2015) Manganese and the Evolution of Photosynthesis. *Orig. Life Evol. Biosph.*, **45**, 351−357.

Goto, K.T., Sekine, Y., Ito, T., Suzuki, K., Anbar, A.D., Gordon, G.W., Harigane, Y., Maruoka, T., Shimoda, G., Kashiwabara, T., Takaya, Y., Nozaki, T., Hein, J.R., Tetteh, G.M., Nyame, F.K. and **Kiyokawa, S.** (2021) Progressive ocean oxygenation at ~2.2 Ga inferred from geochemistry and molybdenum isotopes of the Nsuta Mn deposit, Ghana. *Chem. Geol.,* **567**, 120116.

Gumsley A.P., Chamberlain K.R., Bleeker W., Söderlund U., De Kock M.O., Larsson E.R. and **Bekker A.** (2017) Timing and tempo of the great oxidation event. *Proc. Natl. Acad. Sci.* **114**, 1811−1816,

Halevy, I., Alesker, M., Schuster, E.M., Popovitz-Biro R. and **Feldman, Y.** (2017) A key role for green rust in the Precambrian oceans and the genesis of iron formations. *Nat. Geosci.,* **10**, 135−139.

Haley, B.A., Klinkhammer, G.P. and **McManus, J.** (2004) Rare earth elements in pore waters of marine sediments. *Geochim. Cosmochim. Acta*, **68**, 1265−1279.

Havig, J.R., Hamilton, T.L., McCormick, M., McClure, B., Sowers, T., Wegter, B. and **Kump, L.R.** (2017) Water column and sediment stable carbon isotope biogeochemistry of permanently redox-stratified Fayetteville Green Lake, New York, USA. *Limnol. Oceanog.*, **63**, 570−587.

Heimann, A., Johnson, C.M., Beard, B.L., Valley, J.W., Roden, E.E., Spicuzza, M.J. and **Beukes, N.J.** (2010) Fe, C, and O isotope compositions of banded iron formation carbonates demonstrate a major role for dissimilatory iron reduction in ~2.5 Ga marine environments. *Earth Planet. Sci. Lett.,* **294**, 8−18.

Herndon, E.M., Havig, J.R., Singer, D.M., McCormick, M.L. and **Kump, L.R.** (2018) Manganese and iron geochemistry in sediments underlying the redox-stratified Fayetteville Green Lake. *Geochim. Cosmochim. Acta*, **231**, 50−63.

Hiebert, R.S., Bekker, A., Houlé, M.G. and **Rouxel, O.J.** (2018) Depositional setting of the Late Archean Fe oxide- and sulfide-bearing chert and graphitic argillite in the Shaw Dome, Abitibi greenstone belt, Canada. *Precambrian Res.,* **311**, 98−116.

Hinz, I.L., Nims, C., Theuer, S., Templeton, A.S. and **Johnson, J.E.** (2021) Ferric iron triggers greenalite formation in simulated Archean seawater. *Geology*, **49**, 905−910.

Hummer, D.R., Golden, J.J., Hystad, G., Downs, R.T., Eleish, A., Liu, C., Ralph, J., Morrison, S.M., Meyer, M.B. and **Hazen, R.M.** (2022) Evidence for the oxidation of Earth's crust from the evolution of manganese minerals. *Nat. Commun.*, **13**, 1−7.

James, H.L. (1954) Sedimentary facies of iron-formation. *Econ. Geol.*, **49**, 235-293.

Jiang, C.Z. and **Tosca, N.J.** (2019) Fe^{2+}-carbonate precipitation kinetics and the chemistry of anoxic ferruginous seawater. *Earth Planet. Sci. Lett.,* **506**, 231−242.

Jiang, C.Z., Halevy I. and **Tosca N.J.** (2022) Kinetic isotope effect in siderite growth: Implications for the origin of banded iron formation siderite. *Geochim. Cosmochim. Acta,* **322**, 260−273.

Jiao Y., Kappler A., Croal L.R. and **Newman D.K.** (2005) Isolation and characterization of a genetically tractable photoautotrophic Fe^{2+}-oxidizing bacterium, Rhodopseudomonas palustris strain TIE-1. *App. Environ. Microbiol.*, **71**, 4487−4496.

Johnson, C.M., Beard, B.L., Klein, C., Beukes, N.J. and **Roden, E.E.** (2008) Iron isotopes constrain biologic and abiologic processes in Banded Iron Formation genesis. *Geochim. Cosmochim. Acta,* **72**, 151−69.

Johnson, J.E., Webb, S.M., Thomas, K., Ono, S., Kirschvink, J.L. and **Fischer, W.W.** (2013) Manganese-oxidizing photosynthesis before the rise of cyanobacteria. *Proc. Natl. Acad. Sci.,* **110**, 11238-11243.

Johnson, J.E., Webb, S.M., Ma, C. and **Fischer, W.W.** (2016) Manganese mineralogy and diagenesis in the sedimentary rock record. *Geochim. Cosmochim. Acta,* **73**, 210−231.

Kirschvink, J.L., Gaidos, E.J., Bertani, L.E., Beukes, N.J., Gutzmer, J., Maepa, L.N. and **Steinberger, R.E.** (2000) Paleoproterozoic snowball Earth: Extreme climatic and geochemical global change and its biological consequences. *Proc. Natl. Acad. Sci.,* **97**,

1400−1405.

Klein, C. (2005) Some Precambrian banded iron-formations (BIFs) from around the world: Their age, geologic setting, mineralogy, metamorphism, geochemistry, and origin. *Am. Mineral.*, **90**, 1473–1499.

Kleyenstüber, A.S.E. (1984) The mineralogy of the manganese-bearing Hotazel Formation of the Proterozoic Transvaal Sequence in Griqualand West, South Africa. *Trans. Geol. Soc. S. Afr.*, **87**, 257–272.

Konhauser, K.O., Newman, D.K. and **Kappler, A.** (2005) The potential significance of microbial Fe^{3+} reduction during deposition of Precambrian banded iron formations. *Geobiology*, **3**, 167–177.

Konhauser, K.O., Lalonde, S.V., Amskold, L. and **Holland, H.D.** (2007) Was there really an Archean phosphate crisis? *Science*, **315**, 1234.

Konhauser, K.O., Planavsky, N.J., Hardisty, D.S., Robbins, L.J., Warchola, T.J., Haugaard, R., Lalonde, S.V., Partin, C.A., Oonk, P.B.H., Tsikos, H., Lyons, T.W., Bekker, A. and **Johnson C.M.** (2017) Iron formations: A global record of Neoarchaean to Palaeoproterozoic environmental history. *Earth Sci. Rev.,* **172**, 140−177.

Koschinsky, A., Halbach, P., Hein, J.R. and **Mangini, A.** (1996) Ferromanganese crusts as indicators for paleoceanographic events in the NE Atlantic. *Geol. Rundsch.,* **85**, 567−576.

Koshurba, K.N. and **Johnson, J.E.** (2024) Braunite Synthesized under Simulated Diagenetic Conditions: Implications for the Ancient Manganese Cycle. *ACS Earth Space Chem.*, **8**, 2346-2361.

Kuleshov, V. and **Maynard, J.B.** (eds) (2016) Isotope Geochemistry: The Origin and Formation of Manganese Rocks and Ores. *Elsevier,* 427pp.

Kurzweil, F., Wille, M., Gantert, N., Beukes, N.J. and **Schoenberg, R.** (2016) Manganese oxide shuttling in pre-GOE oceans–evidence from molybdenum and iron isotopes. *Earth Planet. Sci. Lett.,* **452**, 69−78.

Lantink, M.L., Oonk, P.B., Floor, G.H., Tsikos, H. and **Mason, P.R.D.** (2018) Fe isotopes of a 2.4 Ga hematite-rich IF constrain marine redox conditions around the GOE. *Precambrian Res.*, **305**, 218−235.

Lantink, M.L., Davies, J.H.F.L., Mason, P.R.D., Schaltegger, U. and **Hilgen, F.J.** (2019) Climate control on banded iron formations linked to orbital eccentricity. *Nat. Geosci.,* **12**, 369−374.

Lantink M.L., Lenstra W.K., Davies J.H.F.L., Hennekam R., Martin D.McB., Mason P.R.D., Reichart G.-J., Slomp C.P. and **Hilgen F.J.** (2023) Precessional pacing of early Proterozoic redox cycles. *Earth Planet. Sci. Lett.,* **610**, 118117.

Liu, W., Hao, J., Elzinga, E.J., Piotrowiak, P., Nanda, V., Yee, N. and **Falkowski, P.G.** (2020) Anoxic photogeochemical oxidation of manganese carbonate yields manganese oxide. *Proc. Natl. Acad. Sci.,* **117**, 22698−22704.

Lyons, T.W., Reinhard, C.T. and **Planavsky, N.J.** (2014) The rise of oxygen in Earth's early ocean and atmosphere. *Nature*, **506**, 307−315.

Madison, A.S., Tebo, B.M., Mucci, A., Sundby, B. and **Luther, G.W.** (2013) Abundant porewater Mn^{3+} is a major component of the sedimentary redox system. *Science*, **341**, 875−878.

Maliva, R.G., Knoll, A.H. and **Simonson, B.M.** (2005) Secular change in the Precambrian silica cycle: insights from chert petrology. *Geol. Soc. Am. Bull.*, **117**, 835−845.

Maynard, J.B. (2010). The Chemistry of Manganese Ores through Time: A Signal of Increasing Diversity of Earth-Surface Environments. *Econ. Geol.,* **105**, 535−552.

Mhlanga, X.R., Tsikos, H., Lee, B., Rouxel, O.J., Boyce, A.C., Harris, C. and **Lyons, T.W.** (2023) The Palaeoproterozoic Hotazel BIF-Mn Formation as an archive of Earth's earliest oxygenation. *Earth Sci. Rev.*, **240**, 104389.

Miyano, T. and **Beukes, N.J.** (1987) Physicochemical environments for the formation of quartz-free manganese oxide ores from the early Proterozoic Hotazel formation, Kalahari Manganese field, South Africa. *Econ. Geol.,* **82**, 706−718.

Miyano, T. and **Beukes, N.J.** (1997) Mineralogy and petrology of the contact metamorphosed amphibole asbestos-bearing Penge iron formation, eastern Transvaal, South Africa. *J. Petrol.*, **38**, 651−676.

Mloszewska A.M., Mojzsis S.J., Pecoits E., Papineau D., Dauphas N. and **Konhauser K.O.** (2013) Chemical sedimentary protoliths in the >3.75Ga Nuvvuagittuq Supracrustal Belt (Québec, Canada). *Gondwana Res.*, **23**, 574−594,

Morey, G.B., Southwick, D.L. and **Schottler,**

S.P. (1991) Manganiferous Zones in Early Proterozoic Iron-Formation in the Emily District, Cuyuna Range, East-Central Minnesota, Minnesota. *Minnesota Geological Survey Report of Investigations,* **39**, 42p.

Mücke A., Dzigbodi-Adjimah K. and **Annor A.** (1999) Mineralogy, petrography, geochemistry and genesis of the Paleoproterozoic Birimian manganese-formation of Nsuta/Ghana. *Miner. Depos.*, **34**, 297−311

Murray, J.W., Dillard, J.G., Giovanoli, R., Mores, H. and **Stumm, W.** (1985) Oxidation of Mn^{2+}: initial mineralogy, oxidation state and ageing. *Geochim. Cosmochim. Acta,* **49**, 463−470.

Nakada, R., Takahashi, Y. and **Tanimizu, M.** (2016) Cerium stable isotope ratios in ferromanganese deposits and their potential as a paleo-redox proxy. *Geochim. Cosmochim. Acta*, **181**, 89−100.

Namgung, S., Chon, C.-M. and **Lee, G.** (2018) Formation of diverse Mn oxides: a review of biogeochemical processes of Mn oxidation. *Geosci. J.*, **22**, 373−381.

Nel, C.J., Beukes, N.J. and **De Villiers, J.P.R.** (1986) The Mamatwan manganese mine of the Kalahari manganese field, in: Anhaeuser, C.R., and Maske, S., eds., *Mineral. deposits. southern. Africa: Geological Society of South Africa.*,**1**, 963−978.

Nims, C. and **Johnson, J.E.** (2022) Exploring the secondary mineral products generated by microbial iron respiration in Archean ocean simulations. *Geobiology*, **20**, 743−763.

Nke, A.Y., Tsikos, H., Mason, P.R.D., Mhlanga, X.R. and **Tostevin, R.** (2024) A seawater origin for greenalite in iron formation. *Earth. Planet. Sci. Lett.,* **643**, 118917.

Nutman, A.P., Bennett, V.C. and **Friend, C.R.L.** (2017) Seeing through the magnetite: Reassessing Eoarchean atmosphere composition from Isua (Greenland) ≥3.7 Ga banded iron formations. *Geosci. Front.*, **8**, 1233−1240.

Oonk, P.B.H., Mason, P.R.D., Tsikos, H. and **Bau, M.** (2018) Fraction-specific rare earth elements enable the reconstruction of primary seawater signatures from iron formations. *Geochim. Cosmochim. Acta*, **238**, 102−122.

Oonk, P.B.H., Tsikos, H., Mason, P.R.D., Henkel, S., Staubwasser, M., Fryer, L., Poulton, S.W. and **Williams, H.M.** (2017) Fraction-specific controls on the trace element distribution in iron formations: Implications for trace metal stable isotope proxies. *Chem. Geol.*, **474**, 17−32.

Ossa Ossa F., Hofmann A., Wille M., Spangenberg J.E., Bekker A., Poulton S.W., Eickmann B. and **Schoenberg R.** (2018) Aerobic iron and manganese cycling in a redox-stratified Mesoarchean epicontinental sea. *Earth Planet. Sci. Lett.,* **500**, 28−40.

Ossa Ossa F., Hofmann A., Spangenberg J.E., Poulton S.W., Stüeken E.E., Schoenberg R., Eickmann B., Wille M., Butler M. and **Bekker A.** (2019) Limited oxygen production in the Mesoarchean ocean. *Proc. Natl. Acad. Sci.,* **116**, 6647−6652.

Ostrander, C.M., Nielsen, S.G., Owens, J.D., Kendall, B., Gordon, G.W., Romaniello, S.J. and **Anbar, A.D.** (2019) Fully oxygenated water columns over continental shelves before the Great Oxidation Event. *Nat. Geosci.,* **12**, 186−191.

Ostrander, C.M., Heard, A.W., Shu, Y. Bekker, A., Poulton, S.W., Olesen, K.P. and **Nielsen, S.G.** (2024) Onset of coupled atmosphere–ocean oxygenation 2.3 billion years ago. *Nature*, https://doi.org/10.1038/s41586-024-07551-5.

Planavsky, N., Bekker, A., Rouxel, O.J., Kamber, B., Hofmann, A., Knudsen, A. and **Lyons, T.W.** (2010) Rare Earth Element and yttrium compositions of Archean and Paleoproterozoic Fe formations revisited: New perspectives on the significance and mechanisms of deposition. *Geochim. Cosmochim. Acta*, **74**, 6387−6405.

Planavsky, N.J., McGoldrick, P., Scott, C.T., Li, C., Reinhard, C.T., Kelly, A.E., Chu, X., Bekker, A., Love, G.D. and **Lyons, T.W.** (2011) Widespread iron-rich conditions in the mid-Proterozoic ocean. *Nature*, **477**, 448−451.

Planavsky, N., Asael, D., Hofmann, A., Reinhard, T., Lalonde, S.V., Knudsen, A. Wang, X., Ossa Ossa, F., Pecoits, E., Smith, A.J.B., Beukes, N.J., Bekker, A., Johnson, T.M., Konhauser, K.O., Lyons, T.W. and **Rouxel, O.J.** (2014) Evidence for oxygenic photosynthesis half a billion years before the Great Oxidation Event. *Nat. Geosci.*, **7**, 283−286.

Poulton, S.W. and **Canfield, D.E.** (2005) Development of a sequential extraction procedure for iron: implications for iron partitioning in continentally derived

particulates. *Chem. Geol.*, **214**, 209−221.

Poulton, S.W. and **Canfield, D.E.** (2011) Ferruginous conditions: a dominant feature of the ocean through Earth's history. *Elements*, **7**, 107−112.

Rasmussen, B., Muhling, J.R., Suvorova, A. and **Krapež, B.** (2016) Dust to dust: Evidence for the formation of "primary" hematite dust in banded iron formations via oxidation of iron silicate nanoparticles. *Precambrian Res.,* **284**, 49−63.

Rasmussen, B., Muhling, J.R., Suvorova, A. and **Krapež, B.** (2017) Greenalite precipitation linked to the deposition of banded iron formations downslope from a late Archean carbonate platform. *Precambrian Res.*, **290**, 49−62.

Rasmussen B. and **Muhling J.R.** (2018) Making magnetite late again: Evidence for widespread magnetite growth by thermal decomposition of siderite in Hamersley banded iron formations. *Precambrian Res.*, **306**, 64−93.

Rasmussen, B., Muhling, J.R. and **Krapež, B.** (2021) Greenalite and its role in the genesis of early Precambrian iron formations - A review. *Earth Sci. Rev.*, **217**, 103613.

Robbins L.J., Fakhraee M., Smith A.J.B., Bishop B.A., Swanner E.D., Peacock C.L., Wang C.L., Planavsky N.J., Reinhard C.T., Crowe S.A. and **Lyons T.W.** (2023) Manganese oxides, Earth surface oxygenation, and the rise of oxygenic photosynthesis. *Earth Science Rev.*, **239**, 104368.

Riding, R., Fralick, P. and **Liang, L.** (2014) Identification of an Archean marine oxygen oasis. *Precambrian Res.*, **251**, 232−237.

Roy, S. (2006) Sedimentary manganese metallogenesis in response to the evolution of the Earth system. *Earth Sci. Rev.*, **77**, 273−305.

Schad, M., Byrne, J.M., Thomas Arrigo, L.K., Kretzschmar, R., Konhauser, K.O. and **Kappler, A.** (2022) Microbial Fe cycling in a simulated Precambrian ocean environment: Implications for secondary mineral (trans) formation and deposition during BIF genesis. *Geochim. Cosmochim. Acta*, **331**, 165−191.

Schier, K., Bau, M., Smith, A.J.B., Beukes, N.J., Coetzee, L.L. and **Viehmann, S.** (2020) Chemical evolution of seawater in the Transvaal Ocean between 2426 Ma (Ongeluk Large Igneous Province) and 2413 Ma ago (Kalahari Manganese Field). *Gondwana Res.*, **88**, 373−388.

Senger, M.H., Davies. J.H.F.L. Ovtcharova, M., Beukes, N.J., Gumsley, A., Gaynor, S.P., Ulianov, A., Ngobeli, R. and **Schaltegger, U.** (2023) Improving the chronostratigraphic framework of the Transvaal Supergroup (South Africa) through in-situ and high-precision U-Pb geochronology. *Precambrian Res.,* **392**, 107070.

Siahi, M., Tsikos, H., Rafuza, S., Oonk, P.B.H., Mason, P.R.D., Mhlanga, X.R., van Niekerk, D. and **Harris, C.** (2020) Insights into the processes and controls for the absolute abundance and distribution of manganese in Precambrian Iron Formations. *Precambrian Res.*, **350**, 105878.

Slotznick, S.P., Johnson, J.E., Rasmussen, B., Raub, T.D., Webb, S.M., Zi, J.-W., Kirschvink, J.L. and **Fischer, W.W.** (2022) Reexamination of 2.5-Ga "whiff" of oxygen interval points to anoxic ocean before GOE. *Sci. Adv.*, **8**, abj7190.

Smith, A.J.B., Beukes, N.J., Cochrane, J.M. and **Gutzmer, J.** (2023) Manganese carbonate-bearing mudstone of the Witwatersrand-Mozaan succession in southern Africa as evidence for bacterial manganese respiration and availability of free molecular oxygen in Mesoarchaean oceans. S. Afr. J. Geol., **126**, 29−48.

Soo, R.M., Hemp, J., Parks, D.H., Fischer, W.W. and **Hugenholtz, P.** (2017). On the origins of oxygenic photosynthesis and aerobic respiration in Cyanobacteria. *Science,* **355**, 1436−1440.

Sperling, E.A., Wolock, C.J., Morgan, A.S., Gill, B.C., Kunzmann, M., Halverson, G.P., Macdonald, F.A., Knoll, A.H. and **Johnston, D.T.** (2015) Statistical analysis of iron geochemical data suggests limited late Proterozoic oxygenation. *Nature*, **523**, 451−454.

Sun S., Konhauser K.O., Kappler A. and **Li Y.-L.** (2015) Primary hematite in Neoarchean to Paleoproterozoic oceans. *Geol. Soc. Am. Bull.*, **127**, 850−861.

Tebo, B.M., Bargar, J.R., Clement, B.G., Dick, G.J., Murray, K.J., Parker, R.V. and **Webb, S.M.** (2004) Biogenic manganese oxides: properties and mechanisms of formation. *Annu. Rev. Earth Planet. Sci.,* **32**, 287−328.

Thibon, F., Blichert-Toft, J., Tsikos, H., Foden, J., Albalat, E. and **Albarede, F.** (2019) Dynamics of oceanic iron prior to the Great

Oxygenation Event. *Earth Planet. Sci. Lett.,* **506**, 360−370.

Thompson, K.J., Kenward, P.A., Bauer, K.W., Warchola, T., Gauger, T., Martinez, R., Simister, R.L., Michiels, C.C., Llirós, M., Reinhard, C.T., Kappler, A., Konhauser, K.O. and **Crowe, S.A.** (2019) Photoferrotrophy, deposition of banded iron formations, and methane production in Archean oceans. *Sci. Adv.*, **5**, eaav2869.

Tosca, N.J., Guggenheim, S. and **Pufahl, P.K.** (2016) An authigenic origin for Precambrian greenalite: Implications for iron formation and the chemistry of ancient seawater. *Geol. Soc. Am. Bull.,* **128**, 511−530.

Tostevin, R., Shields, G.A., Tarbuck, G.M., He, T., Clarkson, M.O. and **Wood, R.A.** (2016) Effective use of cerium anomalies as a redox proxy in carbonate-dominated marine settings. *Chem. Geol.*, **438**, 146−162.

Tostevin, R. and **Ahmed, I.A.M.** (2023) Micronutrient availability in Precambrian oceans controlled by greenalite formation. *Nat. Geosci.,* **16**, 1188-1193.

Trouwborst, R.E., Clement, B.G., Tebo, B.M., Glazer, B.T. and **Luther, G.W.** (2006) Soluble Mn^{3+} in suboxic zones. *Science,* **313**, 1955−1957.

Tsikos, H., Beukes, N.J., Moore, J.M. and **Harris, C.** (2003) Deposition, diagenesis, and secondary enrichment of metals in the Paleoproterozoic Hotazel iron-formation, Kalahari Manganese Field, South Africa. *Econ. Geol.*, **98**, 1449−1462.

Tsikos, H., Siahi, M., Rafuza, S., Mhlanga, X.R., Oonk, P.B.H., Papadopoulos, V., Boyce, A.J., Mason, P.R.D., Harris, C., Gröcke, D.R. and **Lyons, T.W.** (2022) Carbon isotope stratigraphy of Precambrian iron formations and possible significance for the early biological pump. *Gondwana Res.*, **109**, 416−428.

Walker, J.C.G. (1984) Suboxic diagenesis in banded iron formations. *Nature*, **309**, 340−342.

Wang, X., Planavsky, N.J., Hofmann, A., Saupe, E.E., De Corte, B.P., Philippot, P., LaLonde, S.V., Jemison, N.E., Zou, H., Ossa, F.O., Rybacki, K., Alfimova, N., Larson, M.J., Tsikos, H., Fralick, P.W., Johnson, T.M., Knudsen, A.C., Reinhard, C.T. and **Konhauser, K.O.** (2018) A Mesoarchean shift in uranium isotope systematics. *Geochim. Cosmochim. Acta*, **238**, 438−452.

Wang, C., Robbins, L.J., Planavsky, N.J., Beukes, N.J., Patry, L.A., Lalonde, S.V., Lechte, M.A., Asael, D., Reinhard, C.T., Zhang, L. and **Konhauser, K.O.** (2022) Archean to early Paleoproterozoic iron formations document a transition in iron oxidation mechanisms. *Geochim. Cosmochim. Acta*, **343**, 286−303.

Webb, G.E. and **Kamber, B.S.** (2000) Rare earth elements in Holocene reefal microbialites: A new shallow seawater proxy. *Geochim. Cosmochim. Acta,* **64**, 1557−1565.

Wilmeth, D.T., Corsetti, F.A., Beukes, N.J., Awramik, S.M., Petryshyn, V., Spear, J.R. and **Celestian, A.J.** (2019) Neoarchean (2.7 Ga) lacustrine stromatolite deposits in the Hartbeesfontein Basin, Ventersdorp Supergroup, South Africa: Implications for oxygen oases. *Precambrian Res.*, **320**, 291−302.

Wittkop, C., Swanner, E.D., Grengs, A., Lambrecht, N., Fakhraee, M., Myrbod, A., Bray, A.W., Poulton, S.W. and **Katsev, S.** (2020) Evaluating a primary carbonate pathway for manganese enrichments in reducing environments. *Earth Planet. Sci. Lett.,* **538**, 116201.